Contribution from the Departments of Chemistry, Stanford University, Stanford, California 94305, and Rutgers—The State University of New Jersey, New Brunswick, New Jersey 08903

Spectroscopic and Theoretical Studies of the Unusual EPR Parameters of Distorted Tetrahedral Cupric Sites: Correlations to X-ray Spectral Features of Core Levels

Andrew A. Gewirth,† Susan L. Cohen,† Harvey J. Schugar,*‡ and Edward I. Solomon*†

Received August 28, 1986

X-ray spectral data and self-consistent field–Xα–scattered wave (SCF–Xα–SW) calculations are presented for D_{4h} and D_{2d} $CuCl_4^{2-}$ in order to evaluate specific contributions to the small hyperfine in distorted tetrahedral copper sites and to compare the mechanism of hyperfine reduction in these complexes with that for the blue copper site in plastocyanin. Comparison of the $2p_{3/2}$ XPS data for the two geometries indicates that the extent of delocalization of the $d_{x^2-y^2}$ ground state in the D_{2d} salt is slightly less than in the D_{4h} complex. Multiplet splitting of satellite structure from Cu 3s photoemission shows no change going from D_{4h} to D_{2d} $CuCl_4^{2-}$, indicating that the indirect Fermi contact contribution to the hyperfine from the core Cu 3s level does not change between the two complexes. Analysis of X-ray edge data for Cs_2CuCl_4 (D_{2d}) indicates that there is at most 5.8% $4p_z$ mixed into the ground-state wave function, an amount that is insufficient to explain the reduced hyperfine in this distorted T_d complex. SCF–Xα–SW calculations performed with sphere radii adjusted so that the ground-state wave function fits the experimental g values indicate that ~70% of the reduction in $A_\parallel$ between D_{4h} and D_{2d} comes from increased orbital angular momentum in the ground state of the D_{2d} salt arising from decreased ligand field transition energies. In contrast, increased delocalization relative to D_{4h} $CuCl_4^{2-}$ accounts for most of the reduction in the blue copper proteins. The remaining 30% of the reduction in $A_\parallel$ is associated with a $\sim 50 \times 10^{-4}$ cm^{-1} reduction in Fermi contact between the two salts. Xα calculations of a number of Cu complexes with $<D_{2d}$ symmetry indicate that this reduction is not associated with direct 4s mixing into the half-occupied ground state but is most likely due to increased polarization of the filled totally symmetric valence levels in D_{2d} $CuCl_4^{2-}$ resulting from increased 4s mixing as compared with D_{4h} $CuCl_4^{2-}$. These studies are then extended to include copper sites exhibiting rhombically split g and A values. Single-crystal optical and EPR studies on copper-doped bis(1,2-dimethylimidazole)zinc(II) dichloride ($Zn[Cu](dmi)_2Cl_2$) combined with ligand field and SCF–Xα–SW calculations indicate that the rhombic features in these complexes can be explained through admixture of ~3% d_{z^2} character in the ground-state wave function. Finally, the structurally uncharacterized blue copper protein stellacyanin, which also shows a rhombic EPR spectrum similar to that in $Zn[Cu](dmi)_2Cl_2$, is considered. In contrast to the C_{3v} effective symmetry found in the structurally defined site in plastocyanin, stellacyanin is predicted to have C_{2v} effective symmetry. A ligand field calculation using the plastocyanin site as a starting point indicates that stellacyanin requires a stronger field ligand along the Cu–methionine coordinate to produce the observed d_{z^2} mixing.

1. Introduction

While the electronic structural origin of the EPR parameters in tetragonal copper complexes such as D_{4h} $CuCl_4^{2-}$ is relatively clear,[1,2] the changes in EPR spectral features for complexes distorted to D_{2d} or C_{2v} symmetry remain less well understood. Upon distortion from D_{4h} to D_{2d}-distorted T_d, the parallel hyperfine coupling for $CuCl_4^{2-}$ decreases by over 100×10^{-4} cm^{-1}. An understanding of these changes is particularly important because of their relevance to EPR spectroscopy of blue copper active sites,[3,4] which exhibit small hyperfine couplings ($<70 \times 10^{-4}$ cm^{-1}) and have distorted T_d structures on the basis of high-resolution crystallography reported for plastocyanin by Freeman[5] and azurin by Jensen[6] and Baker.[7] If the D_{2d} site is further distorted to C_{2v} or lower effective symmetry, then in addition to small parallel hyperfine couplings, copper complexes also show splitting in the perpendicular region of the EPR spectrum, i.e. $g_x \neq g_y$ and $A_x \neq A_y$. This rhombic splitting of the spin-Hamiltonian parameters is of particular interest because the EPR spectrum of stellacyanin, a blue copper protein, also shows such splittings. While stellacyanin has not been crystallized and thus no structure is available, spectral studies[8-10] have indicated that it has three ligands in common with plastocyanin (thiolate sulfur and two nitrogens of imidazole); knowledge of additional ligation in stellacyanin is uncertain since it does not contain methionine, which is the fourth ligand at the plastocyanin site.

Hyperfine parameters are related to the electronic structure of the complex via the Abragam and Pyrce[11] hyperfine Hamiltonian

$$\hat{\mathbf{A}} = K\mathbf{S} + P[\mathbf{L} + \xi L(L+1)\mathbf{S} - \tfrac{3}{2}\xi(\mathbf{L}(\mathbf{L}\cdot\mathbf{S}) + (\mathbf{L}\cdot\mathbf{S})\mathbf{L})] \quad (1)$$

where $\xi = {}^2/_{21}$ for d orbitals, $P = g_e g_n \beta_e \beta_n / \langle r^3 \rangle$, K is the Fermi contact term, and the operation is over copper contributions to the spin–orbit-corrected ground-state wave function. For the Cu $d_{x^2-y^2}$ ground state, perturbation theory is used to evaluate eq 1 to obtain

$$A_\parallel = P[\kappa - (4/7)\alpha^2 + (3/7)\Delta g_\perp + \Delta g_\parallel] \quad (2a)$$

$$A_\perp = P[\kappa + (2/7)\alpha^2 + (11/4)\Delta g_\perp] \quad (2b)$$

where α^2 represents the spin density in the half-occupied $d_{x^2-y^2}$ orbital, $\Delta g_{\parallel,\perp}$ are the g shifts from the free electron value of 2.0023, $P = 396 \times 10^{-4}$ cm^{-1} and $\kappa = 0.43$, the last two values being obtained from Hartree–Fock calculations on copper atoms.[12] These equations contain the sum of three contributions: Fermi contact (A_F; $P\kappa$ in the perturbation expression), spin dipolar (A_S; α^2-dependent terms in eq 2) and orbital dipolar (A_L; the Δg terms).

While the expressions in eq 2 work well for a large number of tetragonal copper complexes, they fail when applied to those with D_{2d} or lower symmetry and overestimate $A_\parallel$. In these cases, for example in $Cs_2Zn[Cu]Cl_4$, only use of smaller than accepted values of P and κ give the correct magnitude for $A_\parallel$.

The inability of the expressions in eq 2 to reproduce the experimental hyperfine values for most tetrahedral copper complexes has spurred a number of theoretical and experimental studies with the goal of relating specific electronic structural features in the pseudotetrahedral model complexes and proteins to the small hyperfine. The first analyses[13,14] of the failure of eq 2 to predict

†Stanford University.
‡Rutgers—The State University of New Jersey.

(1) Smith, D. W. *Coord. Chem. Rev.* **1976**, *21*, 93.
(2) Smith, D. W. *J. Chem. Soc. A* **1970**, 3108.
(3) Gray, H. B.; Solomon, E. I. In *Copper Proteins*; Spiro, T. G., Ed.; Wiley: New York, 1981; pp 1–39.
(4) Solomon, E. I.; Penfield, K. W.; Wilcox, D. E. *Struct. Bonding (Berlin)* **1983**, *53*, 1.
(5) Guss, J. M.; Freeman, H. C. *J. Mol. Biol.* **1983**, *169*, 521.
(6) Adman, E. T.; Stenkamp, R. E.; Sieker, L. C.; Jensen, L. H. *J. Mol. Biol.* **1978**, *123*, 35.
(7) Norris, G. E.; Anderson, B. F.; Baker, E. N. *J. Am. Chem. Soc.* **1986**, *108*, 2784.
(8) Rist, G. H.; Hyde, J. S.; Vanngard, T. *Proc. Natl. Acad. Sci. U.S.A.* **1970**, *67*, 79.
(9) Mims, W. B.; Peisach, J. *Biochemistry* **1976**, *15*, 3863.
(10) Roberts, J. E.; Brown, T. G.; Hoffman, B. M.; Peisach, J. *J. Am. Chem. Soc.* **1980**, *102*, 825.
(11) Abragam, A.; Pryce, M. H. L. *Proc. R. Soc. London, A* **1951**, *205*, 135.
(12) Freeman, A. J.; Watson, R. E. In *Magnetism*; Rado, G. T., Suhl, H., Eds.; Academic: New York, 1965; Vol. 2A.
(13) Bates, C. A. *Proc. Phys. Soc., London* **1962**, *79*, 73.
(14) Sharnoff, J. *J. Chem. Phys.* **1965**, *42*, 3383.

0020-1669/87/1326-1133$01.50/0

the reduced $A_\parallel$ in $\sim T_d$ copper complexes required substantial (12%) Cu $4p_z$ mixing into the ground-state wave function. The small hyperfine has also been ascribed to reductions in the Fermi contact term A_F[15] from D_{4h} $CuCl_4^{2-}$. Finally, eq 2 has been said to fail for distorted tetrahedral copper complexes because of substantial contributions to the ground-state angular momentum from chlorine ligands that have large spin–orbit coupling constants,[16-18] necessitating the use of alternative expressions for the Δg-dependent terms. An analysis that systematically evaluates experimentally and theoretically all of the possible contributions to these reduced $A_\parallel$ interactions is lacking, however.

It should also be noted that the contributions cited above for the reduction in $A_\parallel$ in Cs_2CuCl_4 do not appear to be required for the reduced hyperfine in the blue copper site in plastocyanin as calibrated Xα–SW calculations[19] indicate that the reduction is due to the substantially increased delocalization at the site compared with D_{4h} $CuCl_4^{2-}$ (D_{4h} $CuCl_4^{2-}$, 61%; plastocyanin, 42% Cu character). This implies that the major changes in the hyperfine Hamiltonian between plastocyanin and D_{4h} $CuCl_4^{2-}$ are in the spin-dipolar (the $(4/7)\alpha^2$ term in eq 2a) and Fermi contact terms. However, for $CuCl_4^{2-}$ this would also require a 20% increase in delocalization on going from D_{4h} to D_{2d} geometries.

A particular difficulty in the study of these distorted T_d complexes has been evaluation of all the orbital and covalent contributions to the ground-state wave function that can strongly influence the EPR parameters. These factors, in addition to the 4p, spin–orbit and covalent contributions mentioned above, can also include direct 4s mixing into the ground state and indirect spin polarization of core and valence s orbitals. Separation of the effects of each of these terms has proven difficult and in part accounts for the variety of explanations for the reduced $A_\parallel$ in the literature. However, this difficulty can be overcome through detailed calculations calibrated with experiment and the application of complementary spectroscopic methods that can directly probe orbital mixing into the ground state. In particular, high-energy X-ray spectral studies of core levels can provide answers to questions that are not readily accessible by using lower energy methods.

In order to evaluate the various mechanisms of hyperfine reduction in D_{2d} copper complexes, we have performed X-ray photoelectron spectral studies (XPS) on $(CH_3NH_3)_2CuCl_4$ (D_{4h}) and Cs_2CuCl_4 (D_{2d}). The results of these experiments are then used to calibrate ground-state Xα–SW calculations. These calculations are then extended to the hyperfine Hamiltonian in eq 1 with the idea of explicitly evaluation delocalization, angular momentum, and Fermi contact contributions to the hyperfine coupling.

Previous work on C_{2v} distorted copper sites has ascribed the split g values to d_{z^2} mixing into the ground state $d_{x^2-y^2}$ wave function.[20] This analysis did not include contributions of covalency and required,[18] in addition, substantial 4s mixing into the ground state. However, no quantitative analysis of the splitting in the hyperfine parameters has been undertaken. In order to evaluate the additional contributions of lowering symmetry from D_{2d} to the split A and g values in these sites, we have studied the spectral parameters of Cu-doped bis(1,2-dimethylimidazole)zinc(II) dichloride,[21] which exhibits rhombic features similar to those seen in stellacyanin. These features are studied in detail through polarized single-crystal spectroscopy and Xα–SW calculations. Finally, this study is extended to consider the possible structural changes between the structurally defined site in plastocyanin and the site in stellacyanin.

Table I. Structural Parameters for $Cu(NH_3)_2Cl_2$, the C_{2v} Approximation for $Zn[Cu](dmi)_2Cl_2$

atom	position, Bohr x	y	z	radius, bohr	α	l_{max}
outer sphere	0.0000	0.0000	0.4309	6.7510	0.75600	5
Cu	0.0000	0.0000	0.4309	3.1250	0.70697	4
Cl	±3.5767	0.0000	−1.8667	2.5000	0.72325	3
N	0.0000	±3.2057	2.4576	1.8000	0.75197	2
HNA	0.0000	±4.6565	1.2230	1.1771	0.97804	0
HNB	±1.5751	±3.1987	3.5289	1.1771	0.97804	0

2. Experimental Section

Single crystals of Cs_2CuCl_4[22] and $(CH_3NH_3)_2CuCl_4$[23] for XPS studies were prepared by slow evaporation of aqueous or methanolic solutions of the appropriate counterion chloride and $CuCl_2\cdot 2H_2O$. Samples of Cs_2CuCl_4 were mounted on aluminum sample holders with EPO-TEK H21 epoxy and polished with alumina grit prior to insertion in the UHV chamber.[24] The $(CH_3NH_3)_2CuCl_4$ samples were mounted on a small glass slide covered with Aqua-dag colloidal graphite to reduce electron deflection. The samples were covered with cellophane tape, which was removed under vacuum to expose a fresh sample for analysis.[24]

XPS data were obtained with a VG ESCALAB chamber using Mg or Al Kα radiation from a twin-anode, nonmonochromatic source run at 9 kV and 10 mA. Samples were maintained at 160 K and Cu^{2+} reduction was monitored by following the appearance of the chemically shifted Cu^+ or Cu^0 $2p_{3/2}$ line and the disappearance of the characteristic Cu^{2+} satellites, which are not observed in the Cu^+ or Cu^0 spectra. When significant reduction was observed, the sample was removed from the X-ray beam and a fresh sample was used to continue data acquisition. Surface charging in these insulating samples was neutralized with the use of a low-energy electron flood gun directed toward the sample.[24]

Large, well-formed crystals of copper-doped bis(1,2-dimethylimidazole)zinc(II) dichloride[25] ($Zn[Cu](dmi)_2Cl_2$) for EPR and optical studies were prepared by slow evaporation of acetone solutions of 1,2-dimethylimidazole and $ZnCl_2$ in a 2:1 ratio containing $\sim$0.1 mol % $CuCl_2\cdot 2H_2O$. This complex crystallizes in the $P2_1/c$ (monoclinic) space group with four molecules per unit cell. The site symmetry at each Zn(Cu) center is C_1, with the molecule being slightly flattened and twisted relative to an idealized C_{2v} $CuCl_2N_2$ geometry. EPR spectra of $Zn[Cu](dmi)_2Cl_2$ were obtained at X- or Q-band frequencies on a Bruker ER220D spectrometer interfaced with a Nicolet 1180E computer and equipped with an Air Products Helitran pumped helium Dewar and apparatus for measuring crystal rotations. Single-crystal spectra were measured for three different rotations around the crystallographic b and c axes and a third axis, a^*, constructed by careful polishing of the crystal mounted perpendicular to the other two axes. Samples were mounted on the end of quartz rods and inserted into EPR tubes. As these samples show a marked temperature dependence in the EPR experiments,[26] spectra were obtained at 44 K where the features were sharpest. Spectra were calibrated by a speck of DPPH placed close to the sample, while microwave fields were measured with a frequency meter.

Optical spectra were obtained at 77 K with a McPherson RS10 1-m scanning monochrometer equipped with an S20, S1, or a cooled PbS detector. As this crystal is monoclinic, data could be obtained only on faces containing the crystallographic b axis. Extinction directions on the a^*b and bc faces were parallel and perpendicular to b. Crystal spectra were decomposed into molecular spectra through the use of the following relationships:

$$I_x = -0.68I_{a^*} + 1.77I_b - 0.09I_c$$

$$I_y = 1.59I_{a^*} - 0.52I_b - 0.08I_c$$

$$I_z = 0.17I_{a^*} - 0.25I_b + 1.16I_c$$

where the optical and EPR g value coordinate systems (vida infra) are the same.

Standard versions of the Xα–SW code suitably modified for use with the one-electron properties package available through the Quantum Chemistry Program Exchange[27] were used to calculate the electronic structure of the complexes under consideration. For D_{2d} $CuCl_4^{2-}$, the

(15) Yokoi, H. *Bull. Chem. Soc. Jpn.* **1974**, *47*, 3037.
(16) Bencini, A.; Gatteschi, D.; Zanchini, C. *J. Am. Chem. Soc.* **1980**, *102*, 5234.
(17) Bencini, A.; Gatteschi, D. *J. Am. Chem. Soc.* **1983**, *105*, 5535.
(18) Hitchman, M. A. *Inorg. Chem.* **1985**, *24*, 4762.
(19) Penfield, K. W.; Gewirth, A. A.; Solomon, E. I. *J. Am. Chem. Soc.* **1985**, *107*, 4519.
(20) Hitchman, M. A.; Olson, C. D.; Belford, R. L. *J. Chem. Phys.* **1969**, *50*, 1195.
(21) Goodgame, D. M. L.; Goodgame, M.; Rayner-Canhan, G. W. *J. Chem. Soc. A* **1971**, 1923.
(22) Sharnoff, M.; Reiman, C. *J. Chem. Phys.* **1964**, *40*, 8406.
(23) Steadman, J. P.; Willet, R. D. *Inorg. Chim. Acta* **1970**, *4*, 367.
(24) Cohen, S. L., Ph.D. Thesis, MIT, 1986.
(25) Bharadwaj, P.; Potenza, J.; Schugar, H. J., manuscript in preparation.
(26) Gewirth, A. A.; Schugar, H.; Solomon, E. I., unpublished results. This is most likely due to a dynamic Jahn–Teller effect as preliminary Raman data indicate that the host lattice does not undergo a phase transition between room and helium temperatures.
(27) Cook, M.; Case, D. A. *QCPE* **1983**, *3*, 102 (program no. 465).

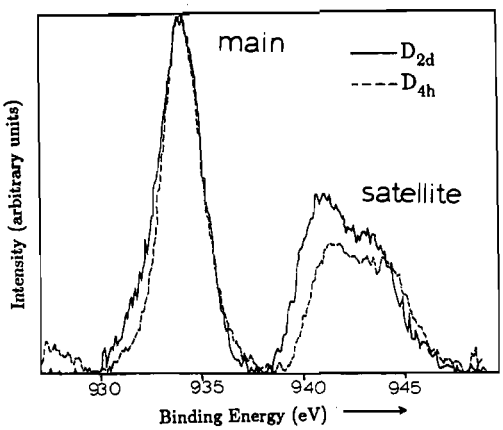

Figure 1. XPS spectra of the $2p_{3/2}$ core level for D_{4h} and D_{2d} $CuCl_4^{2-}$ with main and satellite peaks indicated.

Table II. Parameters Used and Mixing Coefficients Determined for the Configuration Interaction Analysis of $CuCl_4^{2-}$ XPS Satellite Structure

	D_{4h} $CuCl_4^{2-}$	D_{2d} $CuCl_4^{2-}$
I_s/I_m	0.63	0.85
W	8.85	8.20
T	1.95 ± 0.25	1.5 ± 0.30
Q	8.9 ± 0.4	8.9 ± 0.40
Δ	0.88 ± 0.38	0.88 ± 0.38
$\cos^2\theta$, %	61 ± 3	64 ± 3
$\cos^2\theta'$, %	5 ± 1	3 ± 1

structural data for Cs_2CuCl_4[28] were used: the averages of all Cu–Cl bond lengths (2.230 Å), the two small Cl–Cu–Cl angles (100.7°), and the two large Cl–Cu–Cl angles (129.2°). For the D_{4h} geometry, the average (2.265 Å) of the Cu–Cl bond lengths in *N*-methylphenethylammonium copper (II) chloride[29] were used. The idealized structural data for $(enH_2Cl_2)Zn[Cu]Cl_4$ presented in ref 30 were used for Xα calculation of this complex while a C_{2v} approximation with the imidazoles replaced by amines was used for calculation of $Zn[Cu(dmi)_2Cl_2$. Table I gives the coordinates for $Zn[Cu](dmi)_2Cl_2$[25] in this approximation. Other calculations were performed by using geometries described in the text. The α values of Schwarz[31] were used in the atomic region, while the sphere radii were varied in order to fit the experimental g values (vida infra).

3. Results and Analysis

3.1. XPS Spectra. A. $2p_{3/2}$ Satellite Intensities. An experimental estimate of the ground-state delocalization in both D_{2d} and D_{4h} $CuCl_4^{2-}$ is obtained from an analysis of the satellite structure observed in XPS spectra of the Cu core levels. Figure 1 presents $2p_{3/2}$ core level XPS spectra for Cs_2CuCl_4 (D_{2d}) and $(CH_3NH_3)_2CuCl_4$ (D_{4h}). In both of these salts, the main line at 933.9 eV is followed by a satellite peak that is ~8 eV to higher energy. It is clear that the relative satellite intensity in the D_{2d} salt is greater than in the D_{4h} salt. Table II presents the values of the relative intensities, I_s/I_m, and the satellite–main peak splittings, W. These differences in intensities and splittings can be used to calculate the change in delocalization on going from D_{4h} to D_{2d} through the use of the sudden approximation developed by Manne and Aberg[32] and applied by Larsson[33] and Sawatsky[34] to Cu XPS spectra.

In the photoemission process, an electron is ionized from a core level, which in the case of the Cu 2p orbital is split into $2p_{3/2}$ and $2p_{1/2}$ levels through spin–orbit coupling. The complex is thus left with one hole in the 2p level and one hole in the half-occupied

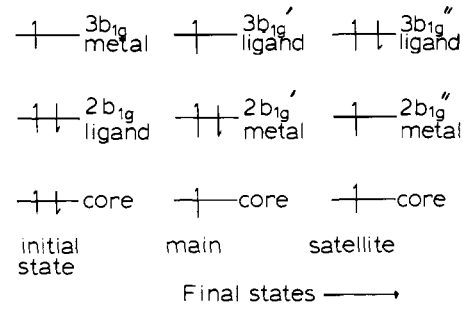

Figure 2. Schematic description of core ionization and satellite formation: left, inital state; middle, resultant lowest energy final state associated with the main peak after ionization of core electron; right, excited final state associated with the satellite.

valence orbital, which corresponds to the main peak in Figure 1. This resultant N – 1 electron ion can relax to further give higher energy satellites (1-electron excited states). In the sudden approximation, the creation of the photoelectron hole occurs rapidly, before the remaining electrons adjust to the new potential. The intensity, I_i, of a given XPS peak, i, corresponding to the main or satellite final state can thus be expressed as

$$I_i = |\langle \Psi_i(N-1)|\Psi_R(N-1)\rangle|^2 \quad (3)$$

where Ψ_i is the relaxed final state and Ψ_R is the initial unrelaxed state with one electron removed. This term implies that only initial and final states with the same symmetry can contribute to satellite formation.

The final-state relaxation occurs because on ionization of a core electron, the effective nuclear charge felt by the valence orbitals increases so that the half-occupied $3b_{1g}$ level, which has mostly metal character in the ground state, becomes mostly ligand-like while the filled $2b_{1g}$ level, at deeper binding energy, becomes more metal centered (middle, Figure 2). The satellite then occurs through a metal-to-ligand charge-transfer "shake-up" from the filled $2b_{1g}$ to the half-occupied $3b_{1g}$ level. The final state, corresponding to the satellite peak, thus has one electron in the 2p core, one electron on the metal, and two electrons in the ligand orbital, which is also the HOMO (right, Figure 2). Note that while there are only two valence levels of b_{1g} symmetry in the D_{4h} complex, four b_2 valence levels occur in the D_{2d} geometry. In this analysis however, we treat only the highest and lowest valence levels, which correlate to the b_{1g} levels in D_{4h} symmetry.

Quantitation of this process and determination of ground-state delocalization can be obtained through use of a configuration interaction type model.[34] Here, the ground-state wave function Ψ_g for the $CuCl_4^{2-}$ molecule is obtained by diagonalizing the energy matrix

$$\begin{vmatrix} \langle\Psi(3d^9)|H|\Psi(3d^9)\rangle - E' & \langle\Psi(3d^9)|H|\Psi(3d^{10}\underline{L})\rangle \\ \langle\Psi(3d^9)|H|\Psi(3d^{10}\underline{L})\rangle & \langle\Psi(3d^{10}\underline{L})|H|\Psi(3d^{10}\underline{L})\rangle - E' \end{vmatrix} = 0 \quad (4)$$

where $\Psi(3d^9)$ and $\Psi(3d^{10}\underline{L})$ represent the one hole–metal and d^{10} metal–one hole–ligand configurations, respectively. Solution gives

$$\Psi_g = \cos\theta|3d^9\rangle - \sin\theta|3d^{10}\underline{L}\rangle \quad (5)$$

as the eigenvector corresponding to the lowest energy configuration with

$$\tan 2\theta = 2T/\Delta \quad (6)$$

where $T = \langle\Psi(3d^9)|H|\Psi(3d^{10}\underline{L})\rangle$ and $\Delta = \langle\Psi(3d^9)|H|\Psi(3d^9)\rangle - \langle\Psi(3d^{10}\underline{L})|H|\Psi(3d^{10}\underline{L})\rangle$. Δ is thus the difference in energies of the two configurations and $x = [(\Delta^2 + 4T^2)^{1/2} - \Delta]/2$ in Figure 3.

Upon creation of the core hole, two possible final states corresponding to the main (Ψ_m) and satellite (Ψ_s) peaks are produced where

$$\Psi_m = \cos\theta'|\underline{c}3d^9\rangle - \sin\theta|\underline{c}3d^{10}\underline{L}\rangle \quad (7)$$

$$\Psi_s = \sin\theta'|\underline{c}3d^9\rangle + \cos\theta'|\underline{c}3d^{10}\underline{L}\rangle \quad (8)$$

(28) McGinnity, J. A. *J. Am. Chem. Soc.* **1972**, *94*, 8406.
(29) Harlow, R. L.; Wells, W. J., III; Watt, G. W.; Simonsen, S. H. *Inorg. Chem.* **1974**, *13*, 2106.
(30) Deeth, R. J.; Hitchman, M. A.; Lehmann, G.; Sachs, H. *Inorg. Chem.* **1984**, *23*, 1310.
(31) Schwarz, K. *Phys. Rev. B: Solid State* **1972**, *5*, 2466.
(32) Manne, R.; Aberg, T. *Chem. Phys. Lett.* **1970**, *7*, 282.
(33) For example, see: Larsson, S. *Phys. Scr.* **1977**, *16*, 378.
(34) van der Lann, G.; Westra, C.; Haas, C.; Sawatsky, G. A. *Phys. Rev. B: Condens Matter* **1981**, *23*, 4369.

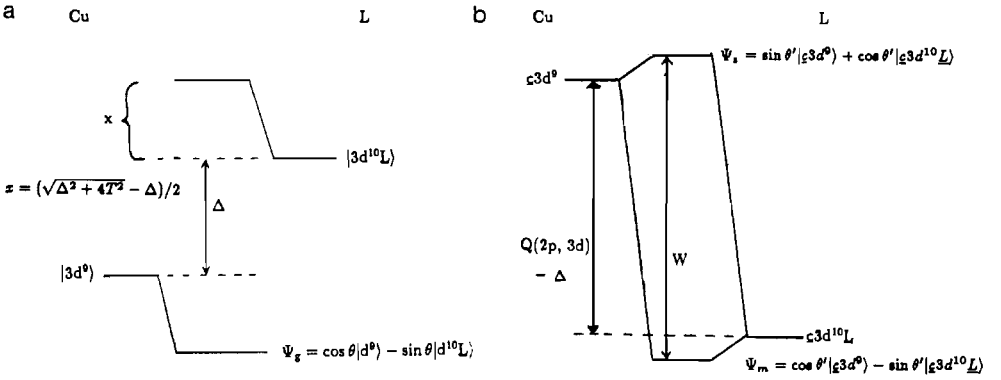

Figure 3. Configuration interaction formalism for analysis of XPS satellite structure. (a) Ground state wave functions are determined completely by the values of T and Δ. (b) Final state: the lowest energy configuration of the core ion, Ψ_m, is depicted here. The shakeup energy (W) is required to promote an electron to the predominantly metal orbital thus giving a final-state wave function, Ψ_s.

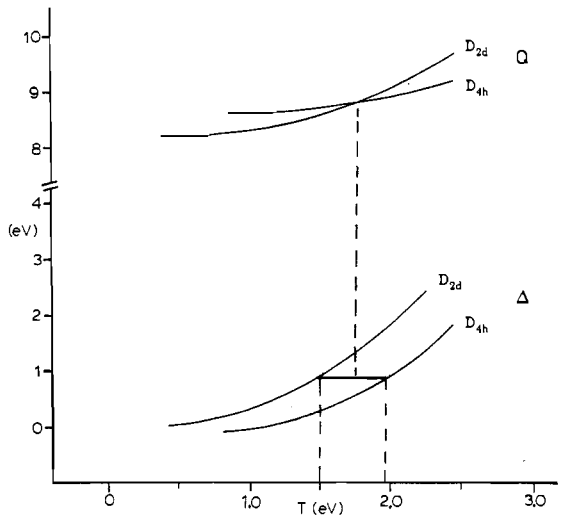

Figure 4. Plot of Q and Δ as functions of T. The lines indicate the region in which Q and Δ are approximately constant, and thus the range of T.

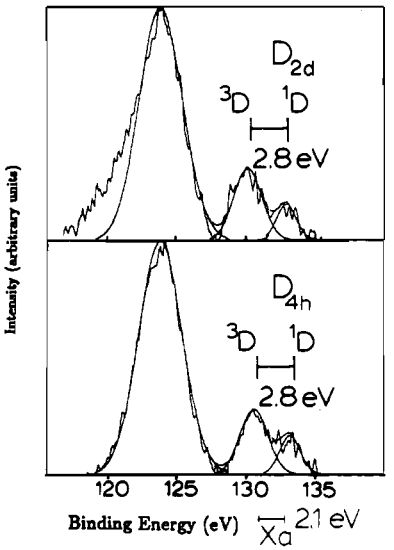

Figure 5. Photoemission spectra from the Cu 3s core level of D_{2d} and D_{4h} $CuCl_4^{2-}$ with the Xα calculated multiplet splitting indicated.

and $\underline{c}$ indicates a hole in the Cu 2p core level. Here, the interaction matrix is constructed in a manner similar to that of the ground-state case in eq 4 with the addition of a term Q to the diagonal energy of the $\underline{c}3d^9$ configuration to account for the interaction of the core hole with the $3d^9$ state (i.e. the increase in effective nuclear charge) and

$$\tan 2\theta' = 2T/(\Delta - Q) \tag{9}$$

with $0 \leq \theta' \leq 90°$. The energy splitting between the main and satellite peaks, W, is thus given by $W = [(\Delta - Q)^2 + 4T^2]^{1/2}$. These interactions are indicated schematically in Figure 3.

Equation 3 combined with eq 5, 7, and 8 leads[34] to the satellite to main peak intensity ratio (I_s/I_m) where

$$\frac{I_s}{I_m} = \left(\frac{\sin\theta'\cos\theta - \cos\theta'\sin\theta}{\cos\theta'\cos\theta + \sin\theta'\sin\theta}\right)^2 = \tan^2(\theta' - \theta) \tag{10}$$

Thus, the intensity ratio is completely determined by the change in the wave function ($\theta' - \theta$) induced upon ionization. As the D_{2d} I_s/I_m ratio is higher than that in D_{4h}, the change in the wave function must be greater in the D_{2d} case.

Given the experimental values I_s/I_m and W in Table II, unique determination of the ground-state wave function requires determination of one of the other parameters T, Q, or Δ in this model. Q and Δ can be expressed in terms of T, and are plotted as a function of T by using the experimental values of W and I_s/I_m in Figure 4. It is reasonable to assume that in both D_{2d} and D_{4h} $CuCl_4^{2-}$ the value of Δ and Q should be approximately constant. Therefore, only the difference in the parameter T determines the differences in ground- and final-state mixing between the two different geometries.

From Figure 4, the requirement that the value of Q be approximately constant for both the D_{4h} and D_{2d} salts is satisfied for T equal to 1.5 ± 0.3 eV for D_{2d} and 1.95 ± 0.25 eV for D_{4h} $CuCl_4^{2-}$ where Q = 8.9 ± 0.4 eV. In all cases, the value of T (for a given Δ) is found to be greater in the D_{4h} molecule by ~0.5 eV than in the D_{2d} molecule. From eq 6, this indicates that the ground-state mixing in the half-occupied $d_{x^2-y^2}$ orbital is greater in D_{4h} than in D_{2d}.

The fraction of Cu d character in the initial state, $\cos^2\theta$, is determined by using the values of Q, Δ, and T from Figure 4 in eq 5 and 6. These results are given in Table II. For the XPS spectra in Figure 1, we find 60 ± 3% d character in the D_{4h} and 63 ± 3% d character in the D_{2d} ground-state wave functions. Thus, it is apparent that distortion of the tetrachlorocuprate anion from D_{4h} to D_{2d} causes only a small increase in the amount of metal character in the ground state of the complex.

Finally, when the values of Q, T, and Δ in Table II are used in eq 9, the final state corresponding to the main line in the photoemission spectrum, Ψ_m, is predicted to have only 2–6% d character for both D_{2d} and D_{4h} $CuCl_4^{2-}$; i.e., it is predominantly a $|\underline{2p}3d^{10}\underline{L}\rangle$ ligand hole state. Alternatively, the satellite corresponds to an almost entirely metal $|\underline{2p}3d^9\rangle$ final state.

B. 3s Multiplet Splitting. An experimental probe of the relative indirect Fermi contact contributions to the hyperfine in D_{2d} and D_{4h} $CuCl_4^{2-}$ is obtained from an analysis of the Cu 3s XPS satellite splittings for the two complexes, which is presented in Figure 5.[35]

(35) Lifetime broadening effects unfortunately obscure the multiplet splitting in the Cu 2s satellite, but the relative splitting here should parallel that of the 3s level.

In both these salts, the main line at ~123 eV is followed by a satellite at ~8 eV to higher binding energy. The satellites are split into two components, with the energy of separation being 2.8 eV in both geometries. This splitting within the satellite can be related to the magnitude of the 3s–3d exchange interaction, which in turn relates to the indirect Fermi contact contribution to the hyperfine.

The origin of the satellite splitting observed in the Cu 3s XPS spectra can be understood by extending the analysis presented in the last section. The satellite final state arising from core level photoemission has almost entirely metal character. As this situation corresponds to one hole in a d orbital and one hole in a Cu core level (Figure 2, right), multiplet splitting corresponding to the energy difference between the singlet and triplet (^{1}D and ^{3}D) final states is expected. Note that this splitting is greatly reduced in the main peak, which corresponds to a ligand hole–metal hole combination (Figure 2, middle). The intensity ratio of the two satellite peaks should be given by the 3:1 triplet–singlet multiplet ratio. Experimentally however, the ratio is found to be closer to 2.5:1, a feature that has been attributed to correlation effects.[36]

The multiplet splitting can be related to the value of the radial integral, G^2, associated with exchange splitting between the 3d and 3s level through the use of the Van Vleck equation[37]

$$\Delta E = \frac{2S + 1}{2l + 1} G^2(3s,3d) \qquad (11)$$

where $l = 2$ and $S = {}^1/_2$ in this case. The proportionality of the multiplet splitting to the exchange integral has been verified over a range of transition-metal complexes.[38] Using eq 11, we obtain $G^2(3s,3d) = 7$ eV for both D_{4h} and D_{2d} $CuCl_4^{2-}$. Significantly, the exchange integral does not change between the D_{4h} and D_{2d} $CuCl_4^{2-}$ complexes.

The exchange integral between the 3s and 3d levels can next be related to the indirect Fermi contact arising from the 3s (and 2s) levels. The core s electrons with the same spin as the electron in the half-occupied $d_{x^2-y^2}$ orbital will experience a different potential than core electrons with opposite spin. This difference in exchange interaction will polarize the core electrons so that the spin population at the nucleus for the same spin core s electrons will be different from that for those with opposite spin. Finally, this population difference gives rise to the Fermi contact interaction through

$$A_F = \frac{8\pi}{3} g_e \beta_e g_N \beta_N \sum_{n=1}^{3} [|\Psi_{ns}\uparrow(0)|^2 - |\Psi_{ns}\downarrow(0)|^2] \qquad (12)$$

where $|\Psi_{ns}\uparrow,\downarrow(0)|^2$ represents the spin density at the nucleus for the same spin and opposite spin core electrons, respectively.

Thus, the multiplet splitting in the copper 3s XPS satellite is directly related to the magnitude of the indirect Fermi contact contribution from the 3s electrons to the hyperfine splitting. As there is no difference in the satellite multiplet splitting going from D_{4h} to D_{2d}, there can be little change in the Fermi contact. As a similar behavior is expected for the 2s and 1s electrons, the indirect core Fermi contact should not significantly contribute to the reduction in $A_\parallel$ on going from D_{4h} to D_{2d} $CuCl_4^{2-}$.

3.2. Xα Calculations of Ground-State Properties. A. *g*-Value Calibration of Covalent Delocalization. Our previous use of an adjustable parameter to fit the Xα–SW calculation to the *g* values and thus estimate covalent delocalization from experiment[19] has led us to alternatively consider the utility of adjusting the ratio of sphere radii to accomplish the same thing completely within the Xα–SW formalism. Previous studies by Bencini and Gatteschi[17] on copper chlorides have indicated that substantial improvement with respect to the ground-state parameters and optical transition energies is obtained by increasing the copper sphere radius over what is calculated through the use of the Norman criteria.[39] This observation is in agreement with other studies,[40,41] which have indicated that enlarging one sphere with respect to another will result in a net flow of charge to the sphere that has been increased, while changing all spheres together will tend to smear out differences between the atomic spheres. These calculations have also indicated[41] that the best results are obtained when the potentials of the atomic spheres measured at the sphere boundries are matched. In this way, it is thought that the electronegativities of all the atoms in the cluster are balanced and that discontinuities inherent in the muffin-tin approach are minimized.[42] We thus systematically adjusted the ratio of the sphere radii in order to (a) adjust the charge distribution so that the Xα charge distribution gave $g_\parallel$ values in agrement with experiment and (b) match the potentials at the sphere boundaries. *g* values were calculated including spin–orbit coupling on metal d and p and ligand p orbitals by using the Xα-calculated charge distribution, analogous to methods developed by McGarvey[43] and Case and Karplus.[44] Spin–orbit coupling was added in a complete calculation, thus avoiding potential inaccuracies arising through the use of the perturbation expressions on systems with low-lying excited states. A matrix element of this calculation is given by

$$M_{ij} = E_{ij}\delta_{ij} + \langle\psi_i|\lambda \mathbf{L}\cdot\mathbf{S}|\psi_j\rangle \qquad (13)$$

where $\psi_{i,j}$ come from the Xα charge distribution, λ is the many electron spin–orbit coupling constant and E_{ii} is an energy such that the eigenvalues from the calculation are the experimentally[45–47] observed energies. Both ligand field and charge-transfer states are included in this calculation with $\lambda_{Cu} = -828$ cm^{-1} and $\lambda_{CL} = -585$ cm^{-1}. The *g* values are then calculated through application of the Zeeman operator, $(\mathbf{L} + 2\mathbf{S})\beta\mathbf{H}$, over the spin–orbit-corrected ground state. Results of these calculations with variable sphere ratios are presented for D_{4h} $CuCl_4^{2-}$ in Table

Table III. Results of *g* Value Calculations, Sphere Radius Potentials and Ground-State Delocalizations for a Number of Different Choices of Cu/Cl Sphere Radii for D_{4h} $CuCl_4^{2-}$

R_{Cu}, bohr	R_{Cl}, bohr	ratio	V(Cu), rydberg	V(Cl), rydberg	ground state % Cu	$g_\parallel$	$g_\perp$
2.40	2.47	0.97	−1.133	−0.825	42	2.144	2.034
2.64	2.54	1.04	−0.953	−0.743	49	2.149	2.035
2.85	2.63	1.08	−0.746	−0.655	57	2.200	2.045
2.85	2.54	1.12	−0.768	−0.685	56	2.192	2.043
2.97	2.54	1.17	−0.660	−0.652	61	2.221	2.050
3.05	2.54	1.20	−0.581	−0.624	64	2.242	2.055

Table IV. Charge Distribution from Adjusted-Sphere Xα Calculation of D_{4h} $CuCl_4^{2-}$

	Cu				Cl			
level	% Cu	% s	% p	% d	% Cl	% s	% p	% d
$3b_{1g}(d_{x^2-y^2})$	61	0	0	99	33	3	93	4
$2b_{2g}(d_{xy})$	80	0	0	100	15	0	95	5
$2e_g(d_{xz,yz})$	74	0	0	100	21	0	98	2
$3a_{1g}(d_{z^2})$	93	5	0	95	2	0	91	9
$1a_{2g}$(nb)	1	0	0	0	87	0	100	0
$4e_u(\pi)$	5	0	23	0	83	0	100	0
$1b_{2u}(\pi)$	2	0	0	0	83	0	100	0
$1e_g(\pi)$	27	0	0	98	60	0	100	0
$2a_{2u}(\pi)$	5	0	75	0	74	0	100	0
$1b_{2g}(\pi)$	22	0	0	99	63	0	99	1
$3e_u(\sigma)$	20	0	83	0	76	1	98	1
$2b_{1g}(\sigma)$	46	0	0	98	51	1	97	2
$2a_{1g}(\sigma)$	32	66	0	28	65	4	94	2

(36) Shirley, D. A. In *Photoemission in Solids*; Cardono, M., Ley, L., Eds.; Springer Verlag: New York, 1978; Vol. 2.
(37) van Vleck, J. H. *Phys. Rev.* **1934**, *35*, 405.
(38) Hufner, S.; Wertheim, G. K. *Phys. Rev. B: Solid State* **1973**, *7*, 2333.
(39) Norman, J. G. *Mol. Phys.* **1976**, *31*, 1191.
(40) Case, D. A.; Cook, M.; Karplus, M. *J. Chem. Phys.* **1980**, *73*, 3294.
(41) Cook, M. R. Ph.D. Thesis, Harvard University, 1981.
(42) Cook, M. R., personal communication.
(43) McGarvey, B. R. *Transition Met. Chem. (N.Y.)* **1966**, *3*, 89.
(44) Case, D. A.; Karplus, M. *J. Am. Chem. Soc.* **1977**, *99*, 6182.
(45) Cassidy, P. J.; Hitchman, M. A. *Inorg. Chem.* **1979**, *18*, 1745.
(46) Ferguson, J. *J. Chem. Phys.* **1964**, *40*, 3406.
(47) Desjardins, S. R.; Penfield, K. W.; Cohen, S. L.; Musselman, R.; Solomon, E. I. *J. Am. Chem. Soc.* **1983**, *105*, 4590.

Table V. Charge Distribution from Adjusted-Sphere Xα Calculation of D_{2d} $CuCl_4^{2-}$

	Cu				Cl			
level	% Cu	% s	% p	% d	% Cl	% s	% p	% d
$5b_2(d_{x^2-y^2})$	71	0	4	94	25	2	95	4
$6e(d_{xz,yz})$	76	0	3	95	20	1	96	3
$2b_1(d_{xy})$	79	0	0	100	16	0	96	4
$4a_1(d_{z^2})$	79	1	0	99	16	0	97	3
$1a_2$(nb)	3	0	0	0	84	0	100	0
$5e(\pi)$	4	0	0	5	83	0	100	0
$3a_1(\pi)$	22	3	0	89	65	0	100	0
$4b_2(\pi)$	11	0	44	41	71	0	100	0
$4e(\pi)$	17	0	11	79	67	0	100	0
$1b_1(\pi)$	24	0	0	97	62	0	99	1
$3e(\sigma)$	33	0	41	46	63	1	97	2
$3b_2(\sigma)$	41	0	13	79	56	1	97	2
$2a_1(\sigma)$	33	74	0	12	64	3	95	2

Table VI. Calculation of Hyperfine Parameters for D_{4h} and D_{2d} $CuCl_4^{2-}$

		g			A^{Cu}, 10^{-4} cm^{-1}		contribn, 10^{-4} cm^{-1}		
		exptl	calcd	% $d_{x^2-y^2}$	exptl	calcd	A_F	A_S	A_L
D_{4h}	∥	2.221	2.221	61	164	−164	−123	−155	+114
	⊥	2.040	2.048		35	−28	−123	+78	+17
D_{2d}	∥	2.435	2.435	67	25	−25	−77	−162	+214
	⊥	2.079	2.112		48	+48	−77	+83	+42

III where it is apparent that the g values are quite sensitive to the sphere radii. The above criteria for the Xα–SW calculation are satisfied with the Cu sphere radius equal to 2.97 bohr and the Cl sphere at 2.54 bohr giving 61% Cu character in the $3b_{1g}$ ground-state orbital. The charge distributions associated with this calculation are presented in Table IV.

This calculation is in essential agreement with our previous results[19] for D_{4h} $CuCl_4^{2-}$ using an adjustable parameter and also with other recent MO[48] and Xα[17] calculations. Application of this approach to the D_{2d} $CuCl_4^{2-}$ salt gives 67.5% Cu $d_{x^2-y^2}$ character with a Cu sphere radius of 3.110 bohr and a Cl radius of 2.490 bohr. The charge distribution is shown in Table V. Thus these Xα calculations indicate that the D_{2d} salt has more metal character in the half-occupied orbital than the square-planar complex, in essential agreement with the $2p_{3/2}$ XPS results presented above.

Having established that the adjusted spheres Xα calculation, fit to the g values, describes the experimental trend in delocalization going from D_{4h} to D_{2d} $CuCl_4^{2-}$, it is now possible to evaluate the spin- and orbital-dipolar terms in the hyperfine Hamiltonian at a reasonable level of confidence. Results of this calculation are presented in Table VI.

B. Spin-Dipolar Contribution to the Hyperfine. The first term in eq 1 to be considered is the spin-dipolar term. There are two ways of evaluating this term from the Xα output. The first way is through explicit evaluation of the dipolar operator, $\mathbf{A}_D$, over the spin–orbit-corrected Xα charge distribution where

$$\mathbf{A}_D = P\xi L(L+1)\mathbf{S} - P\left[\frac{3}{2}\xi(\mathbf{L}(\mathbf{L}\cdot\mathbf{S}) + (\mathbf{L}\cdot\mathbf{S})\mathbf{L})\right] \quad (14)$$

with P and ξ defined previously and the operator evaluated only over the copper center. In the perturbation experiment for $A_\parallel$ in eq 2, this term reduces to $P[(-4/7)\alpha^2 + (3/7)\Delta g_\perp]$. In the calculations presented here, the operator in eq 14 is evaluated over the spin–orbit-corrected ground-state wave function, and the results are partitioned into two terms corresponding to the two terms in the perturbation expression. The first term is presented as A_S in Table VI, while the second term, which reduces to $(3/7)\Delta g_\perp$ in the perturbation expression, is included with the orbital terms considered below. While the sum of these two contributions is traceless, A_S in Table VI is not necessarily so. In addition to the Xα charge distribution, calculation of this term requires evaluation of the $1/r^3$ operator over the Xα wave function. Since the value of $\langle 1/r^3\rangle$ is sensitive to the region close to the copper center, and it is this region in which the numerically solved scattered-wave solution is thought to be best,[41] it is expected that Xα computation of this term will be relatively accurate. For the $^{63}Cu/^{65}Cu$ natural abundance average we obtain in the D_{4h} calculation $P_d = 447 \times 10^{-4}$ cm^{-1} while for the D_{2d} salt we get $P_d = 423 \times 10^{-4}$ cm^{-1}. These results are in broad agreement with those obtained previously[17] with different sphere radii. The D_{2d} value is smaller than that for D_{4h} because of the large Cu sphere radius used in the D_{2d} case. Finally, it is possible to use the calculated values of $\langle 1/r^3\rangle$ to approximate the spin–orbit coupling constant through[49]

$$\lambda \cong -\frac{e^2\hbar^2 Z'}{2m^2c^2}\langle r^{-3}\rangle \quad (15)$$

where Z' is the effective nuclear charge on the copper. Although this equation does not correctly include exchange, for both the D_{2d} and D_{4h} cases we calculate a spin–orbit coupling constant very close to the free ion value of −828 cm^{-1} (D_{4h}, −829 cm^{-1}; D_{2d}, −832 cm^{-1}), which supports the magnitude of $\langle 1/r^3\rangle$ used in the calculation of P.

Application of the operator in eq 14 to the respective charge distributions gives $A_{S\parallel} = -155 \times 10^{-4}$ cm^{-1} and $A_{S\perp} = +78 \times 10^{-4}$ cm^{-1} for D_{4h} $CuCl_4^{2-}$ while for D_{2d} $CuCl_4^{2-}$ we find $A_{S\parallel} = -162 \times 10^{-4}$ cm^{-1} and $A_{S\perp} = +83 \times 10^{-4}$ cm^{-1}, which are in Table VI. The parallel contribution for the D_{2d} salt is slightly larger in magnitude due to the increased metal character (which however is somewhat offset by the reduction in P).

An alternative method of evaluating the dipolar contribution is through direct numerical integration[40] of the spin-dipolar operator over the Xα wave function on the copper nucleus to give

$$A_{Sq} = \left\langle \frac{3q^2 - r^2}{r^5} \right\rangle (\langle\uparrow\rangle - \langle\downarrow\rangle) \quad (16)$$

Here, $q = x$, y, or z and $\langle\uparrow\rangle$ and $\langle\downarrow\rangle$ are the densities of the majority and minority spins on the copper center, respectively. While this alternative calculation does not use the charge distribution separately from the radial factors in the wave function as in the spin-dipolar term calculation presented above and does not require independent evaluation of P, it does require a spin-unrestricted calculation and thus is somewhat more costly. For both geometries however, the results from eq 16, while neglecting small changes due to spin–orbit effects, are within 3×10^{-4} cm^{-1} of those obtained through evaluation of the spin dipolar part of the Abragam and Pryce Hamiltonian (A_S), lending support to this analysis of the dipolar term and to the use of the Xα charge distribution to calculate the hyperfine. Thus, the spin-dipolar contribution to the hyperfine is roughly the same in both the D_{2d} and D_{4h} salts consistent with the small change in delocalization indicated by the XPS results. Therefore, this term does not contribute to the reduction in $A_\parallel$ from D_{4h} to D_{2d} $CuCl_4^{2-}$.

C. Indirect Orbital Dipolar Contributions to Hyperfine. The second term that can be obtained reasonably accurately from the Xα adjusted-spheres wave function is calculated from the orbital-dipolar operator, $PL\cdot\mathbf{I}$ plus off-diagonal elements of eq 14, which gives a nonzero contribution to the hyperfine through spin–orbit coupling between the ground and excited states. As this mechanism is also the one which causes g values to differ from the spin-only value of 2.0023, it is expected that a procedure that fits the g values (i.e. the sphere radii adjustment presented above) will also do well in calculating this term. Inclusion of spin–orbit coupling into the Xα wave function in a complete calculation including both metal and ligand terms avoids problems arising from neglect of ligand contributions to the angular momentum in the ground state, which have been of concern in the past.[16,18]

The results of calculation of the orbital-dipolar term, A_L, are also included in Table VI. It is apparent that the contribution for $A_\parallel$ in the D_{2d} salt is $\sim 100 \times 10^{-4}$ cm^{-1} more postive than in

(48) Aramburo, J. A.; Moreno, M. *J. Chem. Phys.* **1985**, *83*, 6071.

(49) Blume, M.; Watson , R. E. *Proc. R. Soc. London A* **1962**, *270*, 167.

Table VII. Evaluation of the Four Choices of Sign for the Hyperfine Parameters of D_{2d} $CuCl_4^{2-}$ ($\times 10^{-4}$ cm^{-1}) after Subtracting the Sum of the Orbital and the Spin-Dipolar Terms

	$A_\parallel$	$A_\perp$	$\Delta A_\parallel$	$\Delta A_\perp$	ΔA_{iso}	ΔA_{aniso}	% $4p_z$
case 1	+25	+48	−27	−77	−60	+33	9
case 2	+25	−48	−27	−173	−124	+97	27
case 3	−25	−48	−77	−173	−141	+64	17
case 4	−25	+48	−77	−77	−77	0	0

D_{4h}. This accounts for about 70% of the reduction in $A_\parallel$ on going to D_{2d}. This term was also cited by Hitchman[18] as a major contribution to the small hyperfine in the D_{2d} geometry. However, the adjusted-spheres Xα calculation with spin–orbit coupling added in a complete calculation gives a somewhat less positive result for $A_{L\parallel}$ than does the perturbation calculation used in the earlier studies.

That there is substantially more angular momentum mixed into the ground state in D_{2d} $CuCl_4^{2-}$ than in D_{4h} $CuCl_4^{2-}$ is evident from an inspection of the experimental g values for the two complexes in Table VI. The g values for the D_{2d} salt are substantially larger than those for D_{4h}, which arises because the first excited states spin–orbit mixed into the ground state occur at ~ 5000 cm^{-1} lower in energy in D_{2d} than in D_{4h}.[50]

D. Experimental Evaluation of Additional Hyperfine Contributions: Indirect Fermi Contact and Direct 4s and 4p Mixing. The remaining term in the hyperfine Hamiltonian in eq 1 is due to the Fermi contact contribution. The magnitude of this term can be estimated from experiment in the D_{4h} case by subtracting the sum of the spin- and orbital-dipolar terms calculated thus far (-41×10^{-4} cm^{-1} for $A_\parallel$ and $+94 \times 10^{-4}$ cm^{-1} for $A_\perp$) from the experimental hyperfine of $|A_\parallel| = 164 \times 10^{-4}$ cm^{-1} and $|A_\perp| = 34 \times 10^{-4}$ cm^{-1}. The value of this remainder depends on the choice of sign taken for the experimental values. While most EPR experiments only allow measurement of the absolute value of the hyperfine components, the presence of substantial quadrupole coupling can give rise to off-axis EPR or ENDOR signals, which enable determination of relative sign. Such experiments have been performed on a number of tetragonal copper complexes,[51-53] and in all cases the parallel and perpendicular hyperfine have the same sign. For D_{4h} $CuCl_4^{2-}$, with both components negative, the remainder is essentially all isotropic and equal to -123×10^{-4} cm^{-1} for $A_\parallel$ and -128×10^{-4} cm^{-1} for $A_\perp$.[54] The average value of -125×10^{-4} cm^{-1} can be treated as an experimental estimate of the Fermi contact contribution to the hyperfine.

In the D_{2d} $CuCl_4^{2-}$ salt, however, there is no direct experimental support for choosing one set of signs for the hyperfine splittings. Table VII thus presents the remainder terms (ΔA) obtained by subtraction of the calculated sum of the orbital- and spin-dipolar components ($A_\parallel = +52 \times 10^{-4}$ cm^{-1}; $A_\perp = +125 \times 10^{-4}$ cm^{-1}) from the D_{2d} experimental hyperfine parameters for the four possible choices of sign. The remainder terms are further divided into anisotropic and isotropic contributions through the use of

$$\Delta A_\parallel = \Delta A_{iso} + \Delta A_{aniso} \quad (17a)$$

$$\Delta A_\perp = \Delta A_{iso} - \frac{1}{2}\Delta A_{aniso} \quad (17b)$$

The remainder term can thus have contributions from both anisotropic and isotropic components to the hyperfine. The four choices in Table VII can be distinguished by the values of ΔA_{aniso} required by this remainder. ΔA_{aniso} is associated with $4p_z$ mixing into the ground state where 1% $4p_z$ mixing gives $\sim 3.6 \times 10^{-4}$ cm^{-1} to A_{aniso}.[55] Case 1, with $A_\parallel > 0$ and $A_\perp > 0$, requires a $+33 \times 10^{-4}$ cm^{-1} value for ΔA_{aniso}, which implies 9% $4p_z$ mixing into the ground state. The second case, with $A_\parallel > 0$ and $A_\perp < 0$, has $\Delta A_{aniso} = +97 \times 10^{-4}$ cm^{-1}. The large value of ΔA_{aniso} requires 27% $4p_z$ mixing into the ground state. In the third case, $A_\perp < 0$ and $A_\perp < 0$, the value of A_{aniso} would require 17% $4p_z$, while in the fourth case, with $A_\parallel < 0$ and $A_\perp > 0$, $\Delta A_{iso} = -77 \times 10^{-4}$ cm^{-1} and $\Delta A_{aniso} = 0$, implying no additional $4p_z$ contribution. Thus, three of the choices of sign would require substantial $4p_z$ mixing into the ground state.

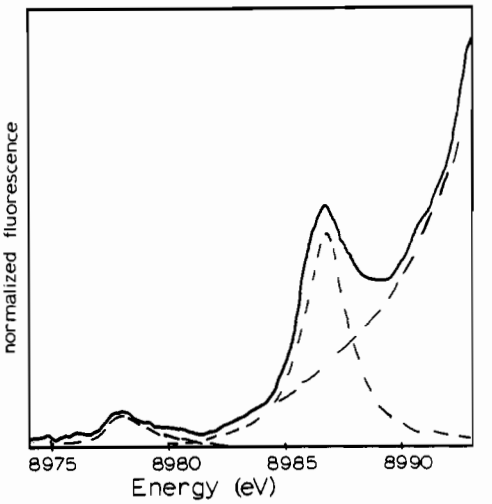

Figure 6. Near-edge-polarized, single-crystal spectra of D_{2d} $CuCl_4^{2-}$ for E parallel to z with resolution of the bands indicated (adapted from Smith[56]).

An experimental probe of the extent of $4p_z$ mixing can be obtained through a preliminary analysis of polarized X-ray edge absorption data[56] for Cs_2CuCl_4 with $\mathbf{E}\parallel z$ shown in Figure 6. The first band at 8979 eV is substantially less intense than the second transition occurring at 8987 eV. For D_{4h} $CuCl_4^{2-}$, the 8979-eV band has been assigned[57] as a 1s to $3d_{x^2-y^2}$ transition made allowed by the quadrupole component of light, which is polarized perpendicular to the z axis. In the D_{2d} spectrum, any $4p_z$ mixing into the ground state will mix electric dipole intensity polarized in the z direction. Thus, all the intensity at 8979 eV in the $\mathbf{E}\parallel z$ polarization reflects admixture of $4p_z$ character into the ground state $d_{x^2-y^2}$ orbital. The 8987-eV band has been assigned[58] as an electric dipole allowed 1s → $4p_z$ transition. The alternative assignment for this band, which we favor, is 1s → 4p simultaneous with a Cl → Cu(II) charge-transfer "shake down" transition made allowed by relaxation due to the increased effective nuclear charge felt by the metal orbitals in the final state (consistent with the Cu 2p XPS results presented above).[59] In this assignment, the area of the 8987-eV band would not be representative of total $4p_z$ intensity but instead would contain some fraction of this character. For either assignment, however, the ratio of the peak area of the 8979-eV transition to that of the 8987-eV band will still give an upper limit of the amount of p_z mixing into the ground-state wave function.

Resolution of each band is shown in Figure 6. The percentage of Lorentzian and Gaussian character used to fit the bands was varied to account for lifetime broadening and monochrometer effects, respectively. Good fits were obtained for between 75 and 50% Lorentzian character with the ratio of the 8979- to 8987-eV bands between 5.4 and 5.8%. Thus any of the hyperfine cases

(50) Solomon, E. I. *Comments Inorg. Chem.* **1984**, *3*, 225.
(51) Duliba, E. P.; Hurst, G. C.; Belford, R. L. *Inorg. Chem.* **1982**, *22*, 577.
(52) Schweiger, A.; Gunthard, Hs. H. *Chem. Phys.* **1978**, *32*, 35.
(53) Brown, T. G.; Hoffman, B. M. *Mol. Phys.* **1980**, *39*, 1073.
(54) If both components are taken to be positive, the remainders are $+205 \times 10^{-4}$ cm^{-1} and -60×10^{-4} cm^{-1} for $A_\parallel$ and $A_\perp$, respectively. This would require an isotropic contribution of $+28 \times 10^{-4}$ cm^{-1} and an anisotropic contribution of $+177 \times 10^{-4}$ cm^{-1} in the parallel region, which would necessitate $\sim 49\%$ p_z mixing into the ground state.
(55) The percentage of $4p_z$ mixing, β, is calculated through the use of $\Delta A_{aniso} = P_p[{}^4/_5\beta]$, where $P_p = \sim 450 \times 10^{-4}$ cm^{-1}.[13]
(56) Smith, T. A., Ph.D. Thesis, Stanford University, 1985.
(57) Hahn, J. E.; Scott, R. A.; Hodgson, K. O.; Doniach, S.; Desjardins, S. R.; Solomon, E. I. *Chem. Phys. Lett.* **1982**, *88*, 595.
(58) Smith, T. A.; Penner-Hahn, J. E.; Berding, M. A.; Doniach, S.; Hodgson, K. O. *J. Am. Chem. Soc.* **1985**, *107*, 5945.
(59) Blair, R. A.; Goddard, W. A. *Phys. Rev. B: Condens. Matter* **1970**, *22*, 2767.
(60) Goodgame, B. A.; Rayner, J. B. *Adv. Inorg. Chem. Radiochem.* **1970**, *13*, 135.

Table VIII. Evaluation of Contributions to Fermi Contact for D_{4h} and D_{2d} $CuCl_4^{2-}$ ($\times 10^{-4}$ cm^{-1})

D_{4h} $CuCl_4^{2-}$			D_{2d} $CuCl_4^{2-}$		
level	contact (% 4s)		level	contact (% 4s)	
1s	−8.6	tot. core contribn −64.9	1s	−9.2	tot. core contribn −70.2
2s	−165.4		2s	−170.3	
3s	+109.1		3s	+109.3	
$1a_{1g}$	−0.1 (0.2)	tot. valence contribn −3.7	$1a_1$	+1.5 (10)	tot. valence contribn +6.1
$2a_{1g}$	−18.8 (14)		$2a_1$	−2.8 (24)	
$3a_{1g}$	+15.2 (5)		$3a_1$	+10.8 (0.6)	
			$4a_1$	−3.4 (0.8)	
tot.	−68.6 (19)		tot.	−64.0 (35)	

in Table VII that require >5.8% $4p_z$ mixing to explain the reduction in hyperfine from D_{4h} to D_{2d} $CuCl_4^{2-}$ can be eliminated. Substantial $4p_z$ mixing is not responsible for the small hyperfine in D_{2d} $CuCl_4^{2-}$.

Case 4 with $A_\parallel = +25 \times 10^{-4}$ cm^{-1} and $A_\perp = -48 \times 10^{-4}$ cm^{-1} requires that A_{iso} changes by $\sim +48 \times 10^{-4}$ cm^{-1} going from D_{4h} to D_{2d}. As the Cu 3s XPS data indicate that no change in the magnitude of the core level indirect Fermi contact occurs in this distortion, the reduction in Fermi contact must therefore be due to some other mechanism. Since the crystallographic site symmetry of the pseudotetrahedral copper complexes is less than D_{2d}, one possible source for this reduction is a low-symmetry distortion allowing direct 4s mixing into the ground state where ~2.5% 4s mixing would be required in this case.[61] Another source could be an increased contribution through spin polarization of valence 4s containing orbitals. These possibilities are probed through spin-unrestricted Xα calculations presented below.

E. Xα Calculation of Fermi Contact. In order to further probe reduction in the Fermi contact term between D_{4h} and D_{2d} $CuCl_4^{2-}$ the Xα wave function was used to calculate this term in the hyperfine Hamiltonian. Evaluation of the contact contribution is accessible through a spin-unrestricted Xα calculation, results of which are presented in Table VIII. The calculation indicates that the D_{2d} and D_{4h} cases have similar core contributions to the contact term, which are -65×10^{-4} cm^{-1} for D_{4h} and -70×10^{-4} cm^{-1} for D_{2d}. These results are consistent with the 3s XPS results, but the calculated Fermi contact is about 55% of what is required experimentally in the D_{4h} calculation (-125×10^{-4} cm^{-1}, vida supra). This result is in agreement with those of other studies, which have also found that the Xα calculation underestimates the strength of the exchange interaction in the region near the nucleus.[62,63] Alternatively, this calculation does indicate that, in the absence of valence contributions, the indirect contact is approximately the same between D_{4h} and D_{2d} $CuCl_4^{2-}$.

An additional experimental evaluation of the performance of the Xα calculations with respect to Fermi contact comes from calculation of the 3s satellite multiplet splitting (Figure 5) associated with this valence–core electron exchange. As more than one Slater determinant is required to represent the singlet–triplet combination, the transition-state formalism and a spin-unrestricted calculation are used.[64-66] The singlet–triplet splitting energy is calculated by first removing an electron from the Cu 3s core level in a spin unrestricted calculation. Energies (E) from a transition-state calculation to the triplet ($E\uparrow\uparrow$, where both the core and "shake-up" electrons have the same spin) and the $m_s = 0$ mixed singlet–triplet ($E\uparrow\downarrow$) configurations are then found with the singlet–triplet splitting equal to $2(E\uparrow\downarrow - E\uparrow\uparrow)$. For D_{4h} we calculate a splitting of 2.1 eV compared with the experimental value of 2.8 eV. Thus, the Xα calculation also underestimates the multiplet splitting observed experimentally.

To evaluate 4s mixing arising from a low-symmetry distortion of the D_{2d} $CuCl_4^{2-}$ chromophore, additional Xα calculations were undertaken on other possible low symmetry geometries for this site as shown in Figure 7: (a) the C_s symmetry of the neat Cs_2CuCl_4 complex[28]; (b) an idealized C_{2v} geometry for the Cu site in the Zn lattice;[30] (c) a C_2 geometry in which one Cl–Cu–Cl plane was rotated 20° from the perpendicular with respect to the other. Finally, we performed Xα calculations on (d) $(enH_2Cl_2)Zn[Cu]Cl_4$ where a previous analysis required 1.1% 4s mixing to explain the hyperfine[30] and (e) $Zn[Cu](dmi)_2Cl_2$(vide infra), where the C_{2v} symmetry of the copper site allows direct 4s mixing into the ground state. In all cases, the calculated amount of s character in the ground state was less than 0.15% (Table IX), which is an order of magnitude too small to explain the reduction in A_{iso}. The inability of the Xα calculations to give substantial 4s mixing into the ground state does not, however, appear to be inherent in the application of the Xα–SW formalism to copper complexes. Calculations performed on D_{4h} $CuCl_4^{2-}$ are consistent in predicting 5% 4s mixing into the $3a_{1g}$ (d_{z^2}) level of the complex, an amount of mixing that is also required from a completely independent angular overlap analysis of the energy of this level.[67]

The fact that the Xα calculations do not predict substantial 4s mixing into the ground state, despite significant distortions away

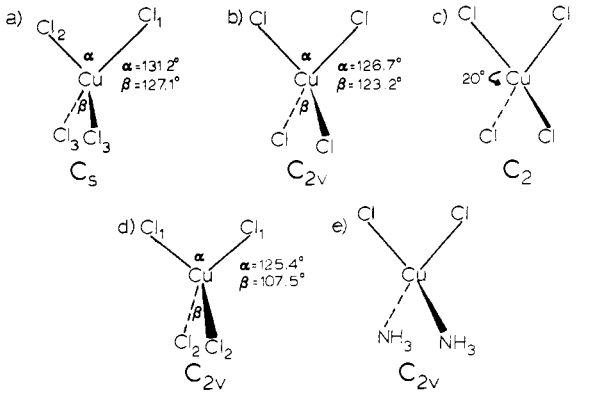

Figure 7. Geometries of low-symmetry copper complexes: (a) $CuCl_4^{2-}$ with C_s symmetry ($R(Cl_1–Cu)$ = 2.244 Å, $R(Cl_2–Cu)$ = 2.235 Å, $R(Cl_3–Cu)$ = 2.220 Å); (b) $CuCl_4^{2-}$ with idealized C_{2v} symmetry (R(Cl–Cu) = 2.269 Å); (c) $CuCl_4^{2-}$ with C_2 symmetry where one Cl–Cu–Cl plane is rotated 20° from the perpendicular to the other Cl–Cu–Cl plane (bond angles and distances are the same as in structure b); (d) $CuCl_4^{2-}$ with idealized geometry[30] for $(enH_2Cl_2)Zn[Cu]Cl_4$ ($R(Cl_1–Cu)$ = 2.305 Å, $R(Cl_2–Cu)$ = 2.260 Å); (e) idealized C_{2v} geometry for $Zn[Cu](dmi)_2Cl_2$ (see Table I).

Table IX. Calculation of Fermi Contact for Distorted Copper Complexes Showing Contributions to the Ground-State Wave Function

complex (sym)	% s	% p_z	Fermi contact, 10^{-4} cm^{-1} valence	core
$CuCl_4^{2-}$ (D_{2d})		2.76	+6.1	−70.2
$CuCl_4^{2-}$ (C_{2v})	0.01	3.57	+5.5	−69.2
$Zn[Cu](dmi)_2Cl_2$ (C_{2v})	0.09	3.38	+7.7	−71.8
$(enH_2Cl_2)Zn[Cu]Cl_4$ (C_{2v})	0.15	3.08	+8.0	−71.7
$CuCl_4^{2-}$ (D_{4h})			−3.7	−64.9

(61) The percentage of 4s mixing is calculated from %4s = $\Delta A_{iso}/1680$ where 1680×10^{-4} cm^{-1} is the hyperfine contribution from direct 4s mixing.[60]
(62) Arratia-Perez, R.; Case, D. A. *J. Chem. Phys.* **1983**, *79*, 4939.
(63) Wilson, T. M.; Wood, J. H.; Slater, J. C. *Phys. Rev. A* **1970**, *2*, 620.
(64) Bagus, P. S.; Bennett, B. I. *Int. J. Quantum Chem.* **1975**, *9*, 143.
(65) Tse, J. S. *J. Chem. Phys.* **1980**, *73*, 3015.
(66) Bristow, D. J.; Tse, J. S.; Bancroft, G. M. *Phys. Rev. A* **1982**, *25*, 1.
(67) Smith, D. W. *Inorg. Chem. Acta* **1977**, *22*, 107.

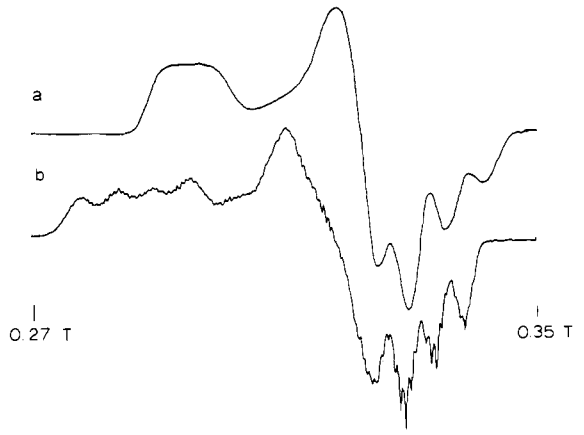

Figure 8. 44 K EPR spectrum of $Zn[Cu](dmi)_2Cl_2$ and stellacyanin: (a) Stellacyanin, microwave field = 9.445 GHz; (b) $Zn[Cu](dmi)_2Cl_2$, microwave field = 9.494 GHz.

from D_{2d} symmetry, indicates that 4s mixing into $d_{x^2-y^2}$ should be excluded as the source of the 48×10^{-4} cm^{-1} increase in A_{iso}. However, from Table IX the Xα calculations are consistent in predicting a $\sim+10 \times 10^{-4}$ cm^{-1} increase in the indirect contact contribution arising from the valence levels. This increase is also predicted in calculations where the Cu and Cl sphere radii are not allowed to change on going from D_{4h} to D_{2d}. Thus, the increase in valence contact contribution is not simply a function of choice of sphere radii for the complexes. When the $\sim+10 \times 10^{-4}$ cm^{-1} increase is scaled by the factor of 2 that the Xα is empirically found to underestimate the indirect contact, the valence 4s polarization makes a substantial contribution to the change in A_{iso} between D_{4h} and D_{2d} $CuCl_4^{2-}$. The increase in valence spin polarization appears to be a consequence of increased 4s character in the valence levels (40% total for D_{2d} vs. 20% total for D_{4h}). Thus, the $\sim+48 \times 10^{-4}$ cm^{-1} change in A_{iso} between D_{4h} and D_{2d} is most likely dominantly due to spin polarization of the valence s electrons, and not 4s mixing into the ground state.

Finally, it should be noted from Table IX that Xα calculation of both the D_{2d} and C_{2v} approximations to $CuCl_4^{2-}$ predicts $\sim$3% p_z mixing into the ground state consistent with the observation of some intensity in the 8979-eV band in the z-polarized XAS spectrum in Figure 6. While this amount of mixing is insufficient by itself to account for the entire diminished $A_\parallel$ in going from D_{4h} to D_{2d}, it can account for $\sim 10 \times 10^{-4}$ cm^{-1} of the reduction and thus should not be neglected entirely.

3.3. Spin-Hamiltonian Parameters in Rhombically Distorted Tetrahedral Copper(II) Complexes. The D_{2d} results are next extended to copper complexes, which, in addition to possessing small $A_\parallel$ values relative to D_{4h} $CuCl_4^{2-}$, also show rhombically split g and A parameters. As mentioned in the Introduction, these complexes are especially interesting as models for the rhombic EPR signal observed for the blue copper protein, stellacyanin. Of particular significance here is the $Zn[Cu](dmi)_2Cl_2$ complex whose EPR spectrum is compared with that of stellacyanin in Figure 8. The EPR spectra of the two complexes are qualitatively quite similar. Both have small A_z values (stellacyanin, 35×10^{-4} cm^{-1}; $Zn[Cu](dmi)_2Cl_2$, 65×10^{-4} cm^{-1}) and both show substantial rhombic splitting of the perpendicular g (stellacyanin, $g_x = 2.018$, $g_y = 2.077$, $\Delta g = 0.059$, $g_{\perp,av} = 2.047$; $Zn[Cu](dmi)_2Cl_2$, $g_x = 2.042$, $g_y = 2.144$, $\Delta g = 0.102$, $g_{\perp,av} = 2.093$) and A (stellacyanin, $|A_x| = 57 \times 10^{-4}$ cm^{-1}, $|A_y| = 29 \times 10^{-4}$ cm^{-1}; $Zn[Cu](dmi)_2Cl_2$, $|A_x| = 45 \times 10^{-4}$ cm^{-1}, $|A_y| = 28 \times 10^{-4}$ cm^{-1}) parameters. The two complexes are also similar in that they both possess heterogeneous ligand sets that contain Cl^- or RS^- ligands that form highly covalent bonds with the copper in addition to two imidazoles per copper site.

The highest effective symmetry that allows rhombic splitting appropriate for the $Zn[Cu](dmi)_2Cl_2$ complex is C_{2v}. When the symmetry is lowered from D_{2d} to C_{2v}, the perturbation expressions for the g shifts become[43]

$$\Delta g_x = \frac{-2\lambda k_x^2 (a - 3^{1/2}b)^2}{E_{xz}} \tag{18a}$$

$$\Delta g_y = \frac{-2\lambda k_y^2 (a + 3^{1/2}b)^2}{E_{yz}} \tag{18b}$$

$$\Delta g_z = \frac{-8\lambda k_z^2 a^2}{E_{xy}} \tag{18c}$$

where k_i represents the Steven's orbital reduction factor, a and b are the coefficients of $d_{x^2-y^2}$ and d_{z^2} in the ground state, respectively, and the denominators are transition energies. There are thus three mechanisms that could split g_x and g_y: differences in the transition energies between E_{xz} and E_{yz}, differences in the Steven's reduction factors (i.e. excited-state delocalization) or d_{z^2} mixing into the ground-state wave function. While d_{z^2} mixing and transition energy differences have been studied in $(enH_2Cl_2)Zn[Cu]Cl_4$ by Hitchman,[30] an analysis of delocalization is still required for a detailed understanding of the g value rhombic splitting.

In addition to the g values, the A values in these low-symmetry copper complexes are also split. In parallel with the g values above, the A value expressions become[43]

$$A_x = P_d\left(-K\alpha^2 + \frac{2\alpha^2(a^2 - b^2)}{7} + \frac{4(3^{1/2})\alpha^2 ab}{7} + \Delta g_x - \frac{(3a - 3^{1/2}b)\Delta g_y}{14(a + 3^{1/2}b)} - \frac{\Delta g_z b}{7a} \right) \tag{19a}$$

$$A_y = P_d\left(-K\alpha^2 + \frac{2\alpha^2(a^2 - b^2)}{7} + \frac{4(3^{1/2})\alpha^2 ab}{7} + \Delta g_y - \frac{(3a + 3^{1/2}b)\Delta g_x}{14(a - 3^{1/2}b)} + \frac{\Delta g_z b}{7z} \right) \tag{19b}$$

$$A_z = P_d\left(-K\alpha^2 - \frac{4\alpha^2(a^2 - b^2)}{7} + \frac{(3a - 3^{1/2}b)\Delta g_y}{14(a + 3^{1/2}b)} + \frac{(3a + 3^{1/2}b)\Delta g_x}{14(a - 3^{1/2}b)} + \Delta g_z \right) \tag{19c}$$

where a and b are defined above and Δg_i are the experimental deviations from $g = 2.0023$. Thus, while the splitting in the g values alone could produce splitting in the A values through the orbital dipolar terms, d_{z^2} mixing into the ground state $d_{x^2-y^2}$ wave function acting through the spin-dipolar term can also impart rhombic character. These possiblities are probed through single-crystal EPR and optical spectroscopy.

A. Single-Crystal Results. Representative X- and Q-band single-crystal EPR spectra for $Zn[Cu](dmi)_2Cl_2$ at 44 and 77 K, respectively, are shown in Figure 9. For rotations around the [100] and [010] axes only one signal is observed, while X-band spectra obtained from rotations around the [001] axis show two signals that are resolved at Q-band frequencies. In all cases, the spectra show substantial superhyperfine structure ranging from a five-line pattern at high fields to a complex, multiline signal at higher g values. Hyperfine splittings are clearly resolved except at intermediate g values.

Figure 10 shows the dependence of the g^2 values on rotation angle for the three sets of rotations. Spin Hamiltonian parameters for $Zn[Cu](dmi)_2Cl_2$ were extracted by fitting the rotation data with a curve of the form

$$g^2 = \alpha + \beta \cos 2\theta + \gamma \sin 2\theta \tag{20}$$

The α, β, and γ parameters were then used in the method of Waller and Rogers[68] to obtain the principal values of the $\mathbf{g}^2$ tensor

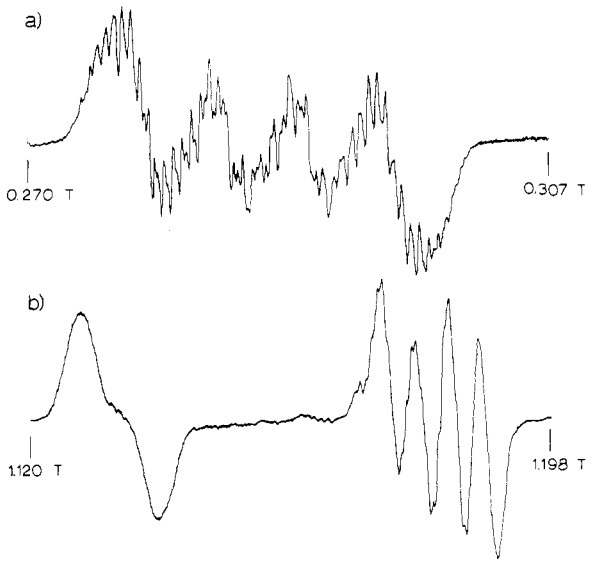

Figure 9. Representative single-crystal EPR spectra for Zn[Cu](dmi)$_2$Cl$_2$: (a) spectrum for rotation around b axis 20° off a^*, close to g_z (T = 44 K, ν = 9.495 GHz); (b) Q-band spectrum of rotation around c axis 45° from b. (T = 77 K, ν = 33.970 GHz). Signals are close to g_y and g_x, respectively.

Table X. Optical and EPR Parameters for Zn[Cu](dmi)$_2$Cl$_2$

param	value
g	2.042, 2.144, 2.365
A, 10^{-4} cm^{-1}	45 ± 1, 28 ± 3, 65 ± 1
Euler angles between A and g, deg	α = −32, β = −14, γ = +26
A^N, 10^{-4} cm^{-1}	max = 8 ± 1; min = 6 ± 1
A^{Cl}, 10^{-4} cm^{-1}	max = 9 ± 1; min = 3 ± 1
$E(^2B_2(d_{yz}) \leftarrow {}^2A_1)$, cm^{-1}	6640
$E(^2B_1(d_{xz}) \leftarrow {}^2A_1)$, cm^{-1}	6920
$E(^2A_1(d_{z^2}) \leftarrow {}^2A_1)$, cm^{-1}	10 250

and the direction cosines that relate the principal values to the rotation axes. Magnetically inequivalent sites in the Zn[Cu](dmi)$_2$Cl$_2$ unit cell give rise to two signals[69] approximately 85° out of phase for rotations around the c axis,[70] which introduces an additional ambiguity into the analysis in that there are now two choices for β and γ for rotations around c. Both possibilities were examined, but only one set gave meaningful results. As each rotation gives three parameters and only a total of six are required to determine the $\mathbf{g}^2$ tensor, this overdetermination is used to obtain starting angle errors, required to make the data internally consistent, for each of the three orthogonal rotations. In all cases, these errors were less than 10°. Two different sets of eigenvalues were obtained from this procedure, but only one of them agreed with the g values obtained from 77 K Q-band powder spectra. Finally, because there are four molecules in the unit cell of the Zn[Cu](dmi)$_2$Cl$_2$ crystal, single-crystal EPR alone can only present four choices for the orientation of the g values. The final choice of eigenvectors was taken to be those that placed the g_z direction closest to the Cl–Cu–Cl bisector, in keeping with ligand field considerations.

The principal g values and their relationship to the Zn[Cu](dmi)$_2$Cl$_2$ molecule are shown in Figure 11 and are listed in Table X. g_z is equal to 2.365 and oriented 4° off the Cl–Cu–Cl bisector and 21° away from the c axis of the crystal. The equatorial g values are split into two components with g_y (=2.144) within 3% of the Cl–Cu–Cl plane while g_x (=2.042) lies close to the N–Cu–N plane.

This same analysis is next applied to the hyperfine values. While hyperfine splittings could be resolved for most of the rotation data, the smallest values observed at fields near g_y in rotations around the c axis could not be determined directly (see Figure 9). Parameters for this rotation were extracted through either a Lorentzian fit of four equally spaced transitions to the unresolved line or through extension of the fit from eq 20 from the larger, resolved splittings in this rotation.

The principal A values along the Euler angles (convention of Rose[71]) relating the $\mathbf{A}^2$ to the $\mathbf{g}^2$ tensor are listed in Table X while their relative orientation is displayed in Figure 11. The A_z and g_z directions are displaced 13°, while the other two A values are rotated approximately 90° with respect to the $\mathbf{g}$ tensor in the sense that the smallest A value (A_y) lies close to the intermediate g value (A_y makes an angle of 9° with g_y).

Finally, almost all of the single-crystal spectra show substantial superhyperfine coupling due to interaction of the nuclear moment of the ligands with the unpaired electron. Thus, the superhyperfine gives insight into the extent of delocalization in the Zn[Cu](dmi)$_2$Cl$_2$ complex. Assuming two equivalent nitrogens and two equivalent chlorines in the complex $(2nI_N + 1)(2nI_{Cl} + 1)$ superhyperfine lines from the ligands should be observed in the perturbation limit. With n = 2, I_N = 1 and I_{Cl} = $^3/_2$; this implies that 35 lines should be observed on every hyperfine peak. Alternatively, if the coupling of one set of ligands is small, then only five or seven lines will be observed for N or Cl, respectively.[72] Figure 9b (right) shows a EPR spectrum obtained with the field close to g_x. Five lines are seen on each hyperfine peak, which implies that the major contribution to the superhyperfine in this orientation is from the nitrogens. Simulation of this spectrum places an upper bound of (3 ± 1) × 10^{-4} cm^{-1} for the chlorine contribution. EPR spectra taken near g_z or g_y are substantially more complex due to superhyperfine contributions from both the Cl and N centers as well as significant quadrupole coupling, which distorts the hyperfine line shapes and complicates analysis. However, simulation gives an upper limit to the Cl superhyperfine of (9 ± 1) × 10^{-4} cm^{-1}. Similarly, the maximum and minimum values of the N superhyperfine coupling are (8 ± 1) × 10^{-4} cm^{-1} and (6 ± 1) × 10^{-4} cm^{-1}. These values are given in Table X.

The experimental superhyperfine parameters are related to delocalization. For both Cl and N, the amount of delocalization is given by[50]

$$C_L^2 = \frac{4}{3}\frac{A_\parallel - A_\perp}{A_{aniso}} + \frac{2}{3}\frac{A_\parallel + 2A_\perp}{A_{iso}} \qquad (21)$$

where C_L^2 is the delocalization and A_{iso} and A_{aniso} are parameters for each ligand type from independent experiment or calculation. $A_\parallel$ and $A_\perp$ are identified with the maximum and minimum values of the superhyperfine tensor, respectively, as the a^* axis of rotation is almost perpendicular to the plane containing the copper and the two chlorines while rotation around b causes the magnetic field to sweep out the plane containing the two nitrogens and the copper. For chlorine,[60] A_{iso} = 1500 × 10^{-4} cm^{-1} while A_{aniso} = 90 × 10^{-4} cm^{-1}, which gives 9.5% unpaired spin character on each chlorine ligand. Similarly, for nitrogen,[60] A_{iso} = 451 × 10^{-4} cm^{-1} and A_{aniso} = 27 × 10^{-4} cm^{-1} giving 6.5% spin character in the ground state for each ligand. Summing gives a total of 33% ligand character in the ground-state orbital, which implies Cu character on the order of 67%. This compares nicely with the 71% Cu character estimated through an adjusted-spheres Xα calculation (vida infra).

Ligand field optical spectra obtained with the electric vector parallel to the a^*, b, and c axes are shown in Figure 12. In order to assign these transitions, the crystal spectra were transformed into a molecular coordinate system with the use of a suitable transformation matrix. As the $\mathbf{g}^2$ and $\mathbf{A}^2$ tensors are essentially colinear, indicating that departures from C_{2v} effective symmetry are not necessary for this complex, the g^2 coordinate system was used to transform the optical data, giving the resolved molecular spectra shown in Figure 12b. The intensity differences in the x and y polarizations relate to differences in mixing of charge-

(68) Waller, W. G.; Rogers, M. T. *J. Magn. Reson.* **1973**, *9*, 92.
(69) Weil, J. A.; Buch, T.; Clapp, J. E. *Adv. Magn. Reson.* **1973**, *6*.
(70) The sites are also inequivalent for rotations around the a^* axis, but experimentally this inequivalence is less than 5°.
(71) Rose, M. E. *Elementary Theory of Angular Momentum*; Wiley: New York, 1957.
(72) Kokoszka, G. F.; Reimann, C. W.; Allen, H. C., Jr. *J. Phys. Chem.* **1967**, *71*, 121.

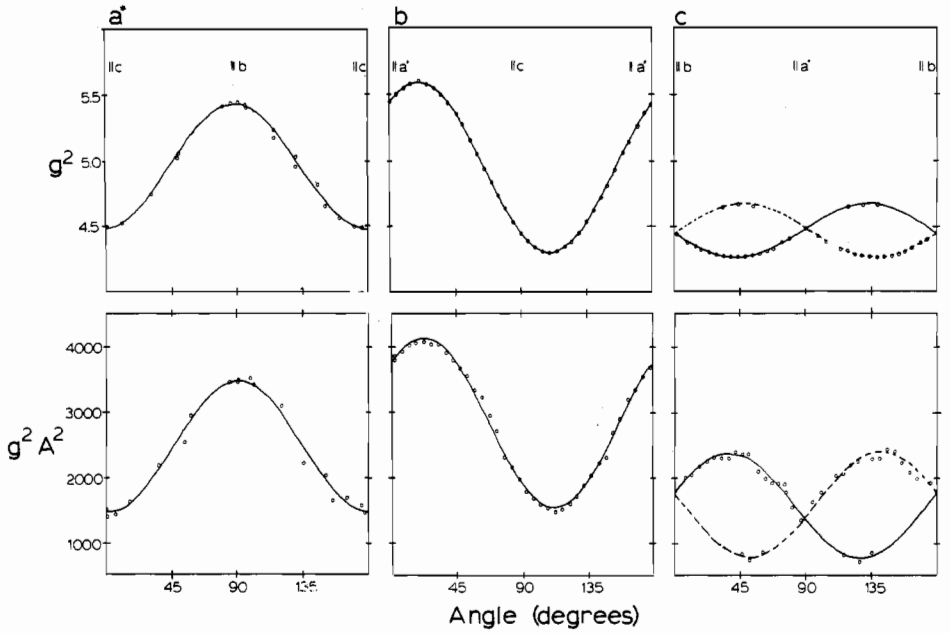

Figure 10. Angular dependence of g^2 (top) and g^2A^2 (bottom) values for Zn[Cu](dmi)$_2$Cl$_2$ for rotations around the a^*, b, and c axes. The circles are experimental points, while the solid line is a least-squares fit of the data. For rotations around c, the dashed g and A value lines correspond.

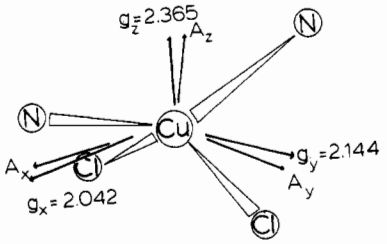

Figure 11. Representation of the Zn[Cu](dmi)$_2$Cl$_2$ site showing directions and magnitudes of the **g** and **A** tensors.

transfer intensity associated with the imidazole and chloride ligands, which are oriented along x and y, respectively. The lowest energy band at 6640 cm^{-1} is y polarized while the 6920-cm^{-1} band has x polarization. Finally, the transition at 10250 cm^{-1} is z polarized. In the C_{2v} point group, these correspond to the $^2B_1(d_{xz}) \leftarrow {}^2A_1$ transition for the band with x polarization, the $^2B_2(d_{yz}) \leftarrow {}^2A_1$ transition for the y-polarized band and the $^2A_1(d_{z^2}) \leftarrow {}^2A_1$ transition for the highest energy ligand field band. The $^2A_2(d_{xy}) \leftarrow {}^2A_1$ transition is not allowed in C_{2v} symmetry and is not observed here. However, this transition is expected to be between 7200 and 8000 cm^{-1} by comparison with the optical data for $(enH_2Cl_2)Zn[Cu]Cl_4$[30] and Cs_2CuCl_4.[46] These results are also included in Table X.

B. Ligand Field Analysis of Rhombic g and A Values. In the absence of d_{z^2} mixing into the ground state the g value shifts in eq 18a,b simplify to

$$\Delta g_x = \frac{\alpha^2\beta_{yz}^2 2\lambda}{\Delta E_{yz}} \tag{22a}$$

and

$$\Delta g_y = \frac{\alpha^2\beta_{xz}^2 2\lambda}{\Delta E_{xz}} \tag{22b}$$

where α^2 is the Cu character in the half-occupied $d_{x^2-y^2}$ orbital, and $\beta_{xz,yz}^2$ and $\Delta E_{xz,yz}$ are the copper character in and the transition energy to the d_{xz} or d_{yz} orbitals, respectively. Thus, the g values could be split by differences in the transition energies to the d_{xz} and d_{yz} levels, the excited state delocalization or, from eq 19 above, d_{z^2} mixing into the ground state. However, the d orbital energies obtained from the optical spectra in Figure 12 would only be sufficient to split the g values by 0.004 around the average of 2.093.

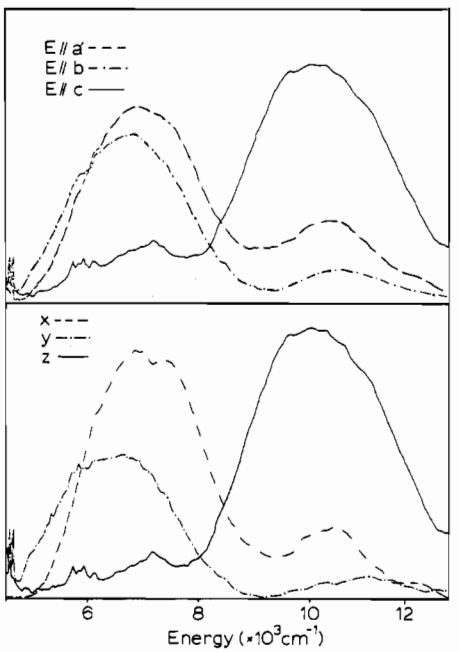

Figure 12. 77 K crystal (top) and molecular (bottom) single-crystal optical spectra for Zn[Cu](dmi)$_2$Cl$_2$.

Therefore, optical transition energy differences are inadequate to explain the split g values.

Both d_{z^2} mixing and changes in excited-state delocalization could provide the origin of the split g values. If all the splitting were attributed to differences in excited state delocalizations, then β_{xz}^2 would have to be 3 times β_{yz}^2. While this difference is unlikely given that the nitrogen character in the ground state is 70% that of the chlorine ligands, it cannot be ruled out. Alternatively, Belford et al.[20] have defined a parameter R_g where

$$R_g = \frac{2(\Delta g_y - \Delta g_x)}{\Delta g_x + \Delta g_y} \tag{23}$$

R_g is thus a measure of the degree of rhombic splitting in the g values and, coupled with the expressions for g_x, g_y, and g_z from eq 19 above, can be written as a function of d_{z^2} mixing into the ground state. A plot of R_g vs. d_{z^2} mixing is shown in Figure 13. R_g is a steep function of the amount of d_{z^2} mixing, which implies

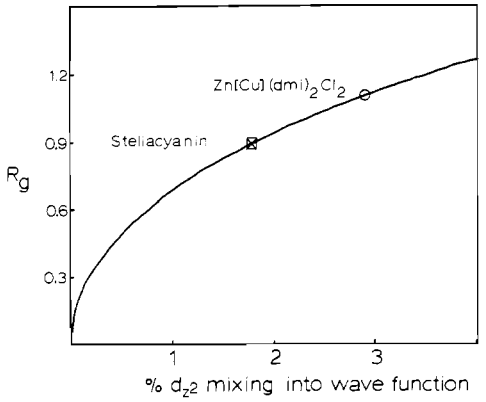

Figure 13. Plot of rhombic splitting in the g values as a function of d_{z^2} mixing into the ground state with the experimental values for Zn[Cu](dmi)$_2$Cl$_2$ and stellacyanin indicated by O and ×, respectively.

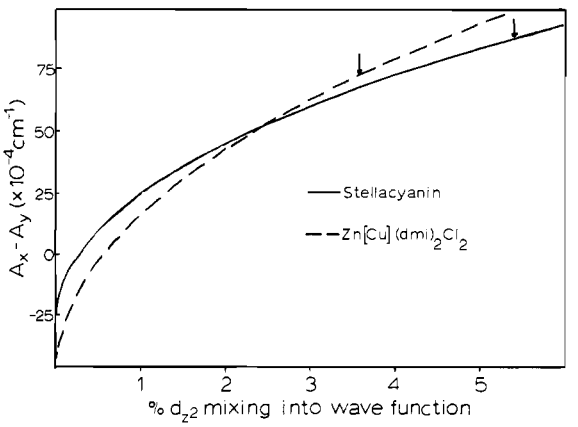

Figure 14. Splitting in A values plotted as a function of d_{z^2} mixing for Zn[Cu](dmi)$_2$Cl$_2$ and stellacyanin. Arrows indicate experimental values associated with each site.

Table XI. Results of g and A Value Calculations for Zn[Cu](dmi)$_2$Cl$_2$

Cu character		g		A^{Cu}, 10^{-4} cm^{-1}		contribn, 10^{-4} cm^{-1}		
		exptl	calcd	exptl	calcd	A_F	A_S	A_L
	x	2.042	2.037	45	+36	-92	+122.9	+5.0
67.6% $d_{x^2-y^2}$	y	2.144	2.138	28	-17	-92	-14.7	+60.0
3.0% d_{z^2}	z	2.365	2.346	65	-65	-92	-135.5	+160.9

that the rhombic splitting should be sensitive to the amount of d_{z^2} mixed into the ground state. For Zn[Cu](dmi)$_2$Cl$_2$, R_g = 1.1, which implies that 2.9% d_{z^2} mixing into the ground-state wave function is sufficient to entirely account for the rhombic splitting.

This analysis can be extended to the rhombically split A values in Zn[Cu](dmi)$_2$Cl$_2$. First, the expressions in eq 19 are used to plot the difference in A along g_x and g_y as a function of d_{z^2} mixing as shown in Figure 14. These plots require the magnitude of P and the ground-state delocalization as well as the experimental g values (Table X) and so are specific to each complex, in contrast to the analysis of the g values. The plots indicate that the rhombic splitting in the A values arises from competition between the split g values, which give $A_x < A_y$, and the spin-dipolar coupling contribution, which splits the A values oppositely. Thus, for a given amount of d_{z^2} mixing, complexes with more splitting in the perpendicular g values will show less splitting in the perpendicular hyperfine.

An additional complication in this analysis arises because of the ambiguity in the signs for A_x and A_y in Table X. For Zn[Cu](dmi)$_2$Cl$_2$ $|A_x - A_y|$ can be either 17 × 10^{-4} or 73 × 10^{-4} cm^{-1}. With no d_{z^2} mixing, $A_x - A_y$ is calculated to be -44 × 10^{-4} cm^{-1}, which is inconsistent with either of these values. Thus, an additional mechanism is required to model the experimental splittings. From Figure 14, either 1% d_{z^2} mixing into the wave function (ΔA = +17; A_x = +44 × 10^{-4} cm^{-1}, A_y = +28 × 10^{-4} cm^{-1}) or 3.2% d_{z^2} mixing (ΔA = +73; A_x = +44 × 10^{-4} cm^{-1}, A_y = -28 × 10^{-4} cm^{-1}) could explain the experimentally observed splittings. Note that the expressions for the rhombic hyperfine in eq 19 coupled with the experimental observation that $|A_x| > |A_y|$ requires A_x to have positive sign. While the presence of substantial superhyperfine coupling precludes the use of quadrupole coupling to experimentally determine the relative signs of A_x and A_y through simulation of off-diagonal EPR signals,[51] the second alternative with ΔA = 73 × 10^{-4} cm^{-1} is consistent with the g value treatment above. Thus, d_{z^2} mixing can provide a consistent explanation of rhombic split g and A values in Zn[Cu](dmi)$_2$Cl$_2$.

C. Xα Calculations of Ground-State Parameters for Rhombic Cu Complexes. In order to further probe the ground-state parameters of Zn[Cu](dmi)$_2$Cl$_2$ and evaluate the d_{z^2} mixing contributions, Xα calculations on Zn[Cu](dmi)$_2$Cl$_2$ have been performed. Results from calculation of ground-state parameters are presented in Table XI, while the ligand field wave functions are given in Table XII.

While the Xα sphere adjustment fit to g_z is not as good for Zn[Cu](dmi)$_2$Cl$_2$ as for the D_{4h} and D_{2d} calculations, the Zn[Cu](dmi)$_2$Cl$_2$ Xα calculation does predict g values consistent with those experimentally obtained. The calculations further indicate that differences in excited-state delocalization are not responsible for the split g values, as the copper characters of the d_{xz} (70%) and d_{yz} (75%) levels are similar. Although both the D_{2d} $CuCl_4^{2-}$ and Zn[Cu](dmi)$_2$Cl$_2$ calculations (Table V and Table XII, respectively) predict similar amounts of ground-state delocalization (~70%) and the transition energy to d_{xy} should be similar in both complexes, g_z is larger in the D_{2d} salt because the d_{xy} level in this complex has greater Cu character (80%) than the d_{xy} level in Zn[Cu](dmi)$_2$Cl$_2$ (57%). The Xα calculation also reproduces the split g values, which arise through 3.0% d_{z^2} mixing into the ground-state wave function. From Table XII, the Xα gives R_g = 1.15 compared with the experimental value of 1.10, which implies that the calcualtion has slightly overestimated the amount of d_{z^2} mixing.

The Xα calculations also reproduce the rhombic split A values in Zn[Cu](dmi)$_2$Cl$_2$. Table XI gives the results of calculation of the spin- and orbital-dipolar terms from the Xα ground-state charge distribution. The A value calculation shows that the rhombic splitting derives from the spin-dipolar term (x, +123 × 10^{-4} cm^{-1}; y, -15 × 10^{-4} cm^{-1}), which is approximately one-third offset by the orbital-dipolar (i.e. Δg value) contribution (x, +5 × 10^{-4} cm^{-1}; y, +60 × 10^{-4} cm^{-1}). This means that the smallest A value in the perpendicular region goes with the largest g value, consistent with the single-crystal results presented above. An important point that supports this analysis should be made by reference to (enH$_2$Cl$_2$)Zn[Cu]Cl$_4$, which has been studied by Hitchman.[30] The large g value splitting in (enH$_2$Cl$_2$)Zn[Cu]Cl$_4$

Table XII. Xα Calculated Ligand Field Levels for Zn[Cu](dmi)$_2$Cl$_2$

	Cu				Cl				N			
level	% Cu	% s	% p	% d	% Cl	% s	% p	% d	% N	% s	% p	% d
$9a_1(d_{x^2-y^2})$	72	0	5	94[a]	21	0	98	1	5	10	89	1
$6b_2(d_{yz})$	75	0	3	95	15	0	98	1	8	9	90	1
$6b_1(d_{xz})$	70	0	6	92	27	0	99	1	0			
$3a_2(d_{xy})$	57	0	0	99	36	0	99	0	0			
$8a_1(d_{z^2})$	78	0	2	97[b]	17	0	99	0	1	3	66	31

[a] 96.5% $d_{x^2-y^2}$, 4.5% d_{z^2}. [b] 11.5% $d_{x^2-y^2}$; 88.5% d_{z^2}.

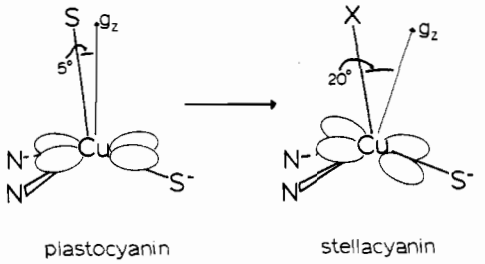

Figure 15. Spectroscopically effective model for ground states of plastocyanin (left) and stellacyanin (right) giving orientation of the $d_{x^2-y^2}$ orbital and the direction of g_z.

Table XIII. Ground-State Parameters for Plastocyanin[72] and Stellacyanin[73]

	plastocyanin	stellacyanin
g_x	2.042	2.018
g_y	2.059	2.077
g_z	2.226	2.287
A_x, 10^{-4} cm^{-1}	−17	+57
A_y, 10^{-4} cm^{-1}	−17	−29
A_z, 10^{-4} cm^{-1}	−63	−35

($g_x = 2.008$, $g_y = 2.201$) results in a smaller A value splitting ($A_x = +71 \times 10^{-4}$ cm^{-1}, $A_y = +43 \times 10^{-4}$ cm^{-1}, $\Delta A = 28 \times 10^{-4}$ cm^{-1}), since the spin-dipolar term is opposed by a large orbital contribution for this complex.

Finally, the Xα calculations indicate that the small A_z value in Zn[Cu](dmi)$_2$Cl$_2$ derives from mechanisms similar to those discussed for D_{2d} $CuCl_4^{2-}$ above. In both cases, the large g values relative to D_{4h} $CuCl_4^{2-}$ contribute substantially to the reduction through the orbital-dipolar term. Since g_z is larger in D_{2d} $CuCl_4^{2-}$, the value of A_z for this complex should be smaller, as is experimentally observed. The hyperfine calculations for Zn[Cu](dmi)$_2$Cl$_2$ and D_{2d} $CuCl_4^{2-}$ also require an additional contribution from a reduced Fermi contact term relative to D_{4h} $CuCl_4^{2-}$. While the A_F value of -90×10^{-4} cm^{-1}, obtained by subtracting the sum of the calculated orbital- and spin-dipolar terms from the experimental value, is somewhat larger than the D_{2d} value of -79×10^{-4} cm^{-1} for this term, it is still 35×10^{-4} cm^{-1} smaller than the D_{4h} value. From Table IX, significant 4s mixing is not found in this or other calculations with low-symmetry sites, and therefore this reduction from the D_{4h} $CuCl_4^{2-}$ A_F value is again attributed to increased spin polarization of the 4s contributions to the valence orbitals. No additional mixings are required relative to the D_{2d} analysis.

D. Stellacyanin. As the above considerations indicate that d_{z^2} mixing into the ground state accounts for the difference in the ground-state parameters between D_{2d} and C_{2v} copper complexes, it is important to examine if the same considerations are involved in correlating the axial EPR parameters in plastocyanin to the rhombic parameters in stellacyanin. Plastocyanin is ligated by a thiolate sulfur of cysteine and two imidazoles of histidine approximately in the g_{xy} plane along with a thioether of methionine in a long 2.9-Å bond oriented 5° off the g_z axis as shown in Figure 15. A previous ligand field calculation indicated that this site has C_{3v} effective symmetry[73] with the long axis along the Cu–S(methionine) bond. While the structure of stellacyanin is unknown, spectroscopic studies have indicated that it shares two imidazoles and a cysteine sulfur in ligation around the copper. However, stellacyanin does not contain methionine, which is the fourth ligand in the plastocyanin site, and thus the nature of ligation at this position is unknown.

A comparison of the ground-state parameters[74,10] for the two proteins is given in Table XIII. The g values in stellacyanin are split by 0.057[10] compared with a splitting in plastocyanin of 0.017, this splitting being due to delocalization over the cysteine thiolate

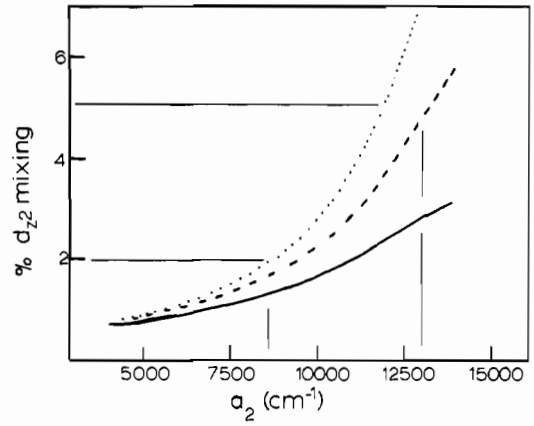

Figure 16. Plot of d_{z^2} mixing into the ground state of stellacyanin as a function of increasing ligand field strength along the Cu–methionine bond direction for three different ratios of ligand field parameters: (—) $\alpha_2 = 4\alpha_4$; (- - -) $\alpha_2 = 2\alpha_4$; (···) $\alpha_2 = 1.5\alpha_4$. Lines give the range of d_{z^2} mixing considered.

p_π orbital (see ref 19 for further discussion). This means that a minimum g values splitting of 0.040 giving an R_g of 0.86 can be associated with d_{z^2} mixing in stellacyanin. From Figure 13, we find that 1.8% $|z^2\rangle$ mixing into the ground-state wave function is sufficient to explain the split g values. Alternatively, if the full $\Delta g = 0.057$ splitting is used, $R_g = 1.24$ and 3.8% d_{z^2} is required.

The hyperfine values of stellacyanin are also split in the perpendicular region with $|A_x| = 75 \times 10^{-4}$ cm^{-1} and $|A_y| = 29 \times 10^{-4}$ cm^{-1}, while splitting in the corresponding values in plastocyanin is too small to be resolved.[75] As with Zn[Cu](dmi)$_2$Cl$_2$, the split g values alone are insufficient to explain either the magnitude of splitting of the A values or the orientation[10] of the $\mathbf{A}^2$ tensor with respect to the $\mathbf{g}^2$ tensor (i.e. the smallest A value along the intermediate g value). From Figure 14, inclusion of d_{z^2} mixing does allow the experimental values to be obtained with either 1.1% d_{z^2} ($\Delta A = 28$; $A_x = +57 \times 10^{-4}$ cm^{-1}, $A_y = +29 \times 10^{-4}$ cm^{-1}; $A_{\perp,av} = +43 \times 10^{-4}$ cm^{-1}) or 5.2% d_{z^2} ($\Delta A = 85$; $A_x = +57 \times 10^{-4}$ cm^{-1}, $A_y = -29 \times 10^{-4}$ cm^{-1}; $A_{\perp,av} = +14 \times 10^{-4}$ cm^{-1}) mixed into the wave function, assuming 42% Cu character in the ground-state wave function.[19] While the percentage of d_{z^2} mixing from the first alternative is somewhat closer to that required from the g values, this would require a shift of 60×10^{-4} cm^{-1} from the plastocyanin $A_\perp$ of -17×10^{-4} cm^{-1}. The alternative possibility with $A_\perp = +14 \times 10^{-4}$ cm^{-1} requires a shift of 31×10^{-4} cm^{-1} from plastocyanin. A smaller shift is prefered from this analysis as this would be consistent with the very limited change in $g_\perp$ between plastocyanin ($g_\perp = 2.051$) and stellacyanin ($g_\perp = 2.047$). Finally, the shift in $A_\parallel$ values between the two sites is largely due to the large g_z for stellacyanin compared with that for plastocyanin.

The calculated range of d_{z^2} mixing into the stellacyanin ground-state wave function can now be used to gain insight into the changes between the bonding in stellacyanin relative to that in plastocyanin. A previous ligand field calculation[73] on plastocyanin indicated that the C_{3v} effective symmetry of the blue site in plastocyanin is rhombically distorted. However, the rhombic distortion occurs in the equatorial plane defined by the two histidine and the cysteine ligands. For this type of rhombic distortion d_{z^2} is not mixed into the ground state because of the small matrix element between the d_{z^2} and $d_{x^2-y^2}$ basis functions. For stellacyanin the above analysis requires between 2 and 5% d_{z^2} mixing into the ground state. It should be noted however that the amount of d_{z^2} mixing from the $\Delta g_{x,y}$ analysis (between 1.8 and 3.8%) is probably more accurate as no assumptions about ground-state delocalization must be made. If one starts with the plastocyanin geometry, this amount of d_{z^2} mixing necessitates increased ligand field strength in a direction perpendicular to the g_{xy} plane, i.e. the z direction,

(73) Penfield, K. W.; Gay, R. R.; Himmelwright, R. S.; Eichman, N. C.; Norris, V. A.; Freeman, H. C.; Solomon, E. I. *J. Am. Chem. Soc.* **1981**, *103*, 4382.
(74) Fee, J. A. *Struct. Bonding (Berlin)* **1983**, *53*, 1.
(75) Roberts, J. E.; Cline, J. F.; Lum, V.; Freeman, H.; Gray, H. B.; Peisach, J.; Reinhammer, B.; Hoffman, B. M. *J. Am. Chem. Soc.* **1984**, *18*, 5324.

Table XIV. Results of Hyperfine Calculation of $A_\parallel$ for D_{4h} and D_{2d} $CuCl_4^{2-}$ and Plastocyanin

complex	g_z	% $d_{x^2-y^2}$	contribn, 10^{-4} cm^{-1} A_F	A_S	A_L
D_{4h} $CuCl_4^{2-}$ (Xα)	2.221	61.0	−123	−155	+114
D_{2d} $CuCl_4^{2-}$ (Xα)	2.435	67.5	−77	−162	+214
D_{2d} $CuCl_4^{2-}$ (pert. theory)	2.435	68.7	−54	−157	+188
plastocyanin	2.226	42	−79	−90	+106

which is within 5° of the Cu–methionine bond direction. Figure 16 gives a plot of ground-state d_{z^2} character as a function of increasing ligand field strength along the Cu–methionine bond in the plastocyanin site geometry. Here, the method of Companion and Komarynsky[76] was used and the ground state was assumed to have 42% Cu character in order to obtain the d_{z^2} mixing into the ground-state wave function. As the identity of this fourth ligand is unknown in stellacyanin and two parameters are required to describe its ligand field, calculations were performed with three different choices for the ratio of the second and fourth power radial integral parameters: $\alpha_2 = 4\alpha_4$; $\alpha_2 = 2\alpha_4$, and $\alpha_2 = 1.5\alpha_4$. The crystal field parameters from our previous crystal field calculation[73] were used for the imidazole and thiolate ligands, which stallacyanin should have in common with plastocyanin. To reproduce the 2–5% d_{z^2} mixing required from analysis of the EPR parameters, an α_2 value between ~9000 and ~12 500 cm^{-1} is necessary. In contrast, α_2 was 4000 cm^{-1} for methionine in plastocyanin ($\alpha_2 = 4\alpha_4$ in this case). Concomitant with the increase in ligand field strength along the Cu–methionine direction, the g_z vector moves ~15° further away from this X–Cu bond where X is the replacement ligand for methionine.[77] Thus, the increase in ligand field strength here means that the site no longer has approximate C_{3v} effective symmetry, as it does in plastocyanin,[73] but rather that the effective site symmetry is closer to C_{2v}. A reasonable estimate for the approximate orientation of the ground-state wave function for stellacyanin is given in Figure 15.

4. Discussion

The XPS and Xα results reported above indicate that ~70% of the reduction in $A_\parallel$ going from D_{4h} to D_{2d} $CuCl_4^{2-}$ is due to increased orbital angular momentum in the ground state of the D_{2d} site, which is also reflected in increased g values in this salt. There is also a remaining contribution to the reduction that is isotropic in character and most likely relates to increased spin polarization of the totally symmetric valence levels in D_{2d}, which contain 4s mixing.

The XPS and edge results provide a probe of various contributions to the ground-state wave function and clearly eliminate some of the previous postulated mechanisms for hyperfine reduction between D_{4h} and D_{2d} $CuCl_4^{2-}$. Analysis of the $2p_{3/2}$ main and satellite peaks provides an independent probe of the relative delocalization between the D_{4h} and D_{2d} $CuCl_4^{2-}$ salts and shows that the change in delocalization between the two complexes is only 6%. The Cu 3s satellite multiplet splitting provides a probe of indirect Fermi contact from the core s electrons, which indicates that the relative contributions do not change between D_{4h} and D_{2d}. Finally, the X-ray edge results indicate that at most 5.8% $4p_z$ mixing is present in the ground state of D_{2d} $CuCl_4^{2-}$. This amount of mixing is insufficient to account for the observed reduction between the two geometries.

The experimentally calibrated results from the Xα calculation can now be compared with the results of perturbation theory (eq 2) where previous interpretations of the hyperfine in D_{2d} have held that these expressions are inadequate to explain the experimental values. Table XIV gives a comparison of the results of the complete calculation of the hyperfine using the Xα charge decomposition and the results from perturbation theory derived from simultaneous solution of eq 2 for α^2 and $P\kappa$ using the experimental values of $A_\parallel = -25 \times 10^{-4}$ cm^{-1} and $A_\perp = +48 \times 10^{-4}$ cm^{-1}. The agreement between perturbation theory and the complete calculation is good. In order to obtain this agreement, however, several factors must be included. Delocalization must be taken into account, and while both the Xα and perturbation theory require a drop in the magnitude of the contact term compared with the -125×10^{-4} cm^{-1} value for D_{4h} $CuCl_4^{2-}$, no substantial drop is necessary in the value of P. The perturbation theory results, in agreement with our analysis, do not require invoking substantial $4p_z$ mixing into the ground-state wave function. Finally, while the perturbation theory expressions do not accurately account for sources of angular momentum other than the copper center, use of the experimental g values to approximate the A_L term results in only a 26×10^{-4} cm^{-1} deviation from the results of complete calculation, which specifically takes the ligands into account.

Table XIV also gives the results from our previous analysis of the hyperfine in the blue copper site in plastocyanin. In plastocyanin, the reduction in $A_\parallel$ derives from reduction of the spin-dipolar term resulting from increased delocalization at the copper site relative to that in D_{4h} $CuCl_4^{2-}$. However, in the D_{2d} salts considered in this paper the major source of reduction in $A_\parallel$ is in the orbital-dipolar term, A_L. The g values in plastocyanin and the square-planar copper chloride salt are similar, and so this cannot be the cause of the reduction in the protein. Further, both the D_{2d} salt and plastocyanin require a $\sim 50 \times 10^{-4}$ cm^{-1} drop in the magnitude of the contact term relative to D_{4h}. While this drop relates primarily to increased spin polarization of the valence contributions of the 4s orbitals in D_{2d}, the increased delocalization in the blue site relative to D_{4h} should also contribute.

In the Cu complexes of C_{2v} effective symmetry, the spectroscopic features can be explained through admixture of around 3% d_{z^2} character into the ground-state wave function. As is the case in the D_{2d} sites, the small A_z derives mostly from the increased g value contributions to the orbital-dipolar terms relative to those to tetragonal copper sites. The d_{z^2} mixing serves to split both the perpendicular g and A values, even in highly covalent sites. In sites of this low symmetry, where 4s mixing is allowed directly into the ground-state orbital, less than 0.2% of this mixing is found through Xα calculation on sites with a wide variety of distortions. As the Xα calculations do well on other small components of the wave function, it is unlikely that the calculations could be over 1 order of magnitude in error here. Thus the reduction in A_F in these C_{2v} sites appears also to be due in large measure to increased valence spin polarization and not direct 4s mixing into the ground state orbital.

The C_{2v} results extended to the blue copper site in stellacyanin indicate that the rhombic splitting seen in the EPR spectrum is due to between 2 and 5% d_{z^2} mixing into the ground state. A ligand field analysis implies that increased ligand field strength at the methionine position relative to plastocyanin can bring about this amount of d_{z^2} mixing. In turn, this increased ligand strength means that in contrast to the C_{3v} effective symmetry in plastocyanin, the stellacyanin site is likely closer to C_{2v} effective symmetry with the $d_{x^2-y^2}$ ground-state orbital significantly rotated relative to that of plastocyanin.

Acknowledgment. We thank Prof. Keith O. Hodgson for preliminary X-ray edge data, Prof. R. Linn Belford for providing EPR simulation programs, Dr. Michael R. Cook for helpful discussions on the Xα calculations, and Stephen V. Didziulis for assistance with the XPS experiments. Funding of this work by the NSF (Grant CHE-82-04841) is gratefully acknowledged. Calculations were (in part) supported by Grant No. CHE-8312693 from the National Science Foundation.

(76) Companion, A. L.; Komarynsky, M. A. *J. Chem. Educ.* **1964**, *41*, 257.
(77) Increasing the ligand field strength along this coordinate also rotates g_x and g_y 15° relative to plastocyanin. In the limit of strict C_{2v} symmetry, this would place to the intermediate g value in the X–Cu–S plane, consistent with the results for Zn[Cu](dmi)$_2$Cl$_2$ where g_y was in the Cl–Cu–Cl plane.